Hindawi
Structural Control and Health Monitoring
Volume 2023, Article ID 5524170, 20 pages
https://doi.org/10.1155/2023/5524170

Research Article

Energy Analysis of a Damped Substructure Outrigger System

Liangkun Liu[1,2] **Ping Tan**[3] **Zhaodong Pan**[1,4] **Bo Di**[1,2] **Shumeng Pang**[1,4] **and Renyuan Qin**[1,5]

[1]*School of Environment and Civil Engineering, Dongguan University of Technology, Dongguan, China*
[2]*Guangdong Provincial Key Laboratory of Intelligent Disaster Prevention and Emergency Technologies for Urban Lifeline Engineering, Dongguan, China*
[3]*School of Civil Engineering, Guangzhou University, Guangzhou, China*
[4]*Dongguan Key Laboratory of Disaster Prevention and Structure Rehabilitation, Dongguan, China*
[5]*Department of Architecture and Civil Engineering, City University of Hong Kong, Hong Kong, China*

Correspondence should be addressed to Zhaodong Pan; pzd0101@126.com

Received 31 May 2023; Revised 17 July 2023; Accepted 2 August 2023; Published 21 September 2023

Academic Editor: Chia-Ming Chang

Copyright © 2023 Liangkun Liu et al. This is an open access article distributed under the Creative Commons Attribution License, which permits unrestricted use, distribution, and reproduction in any medium, provided the original work is properly cited.

A damped outrigger system (DO) has been proposed to enhance the seismic performance, in which links between outriggers and perimeter columns are artificially disconnected and implemented by dampers. Such an operation essentially destroys the structural integrity and becomes a potential threat for structural safety. Moreover, its performance is very sensitive to the stiffness of perimeter columns. In this study, a mega-sub controlled system is employed to propose a novel outrigger system, i.e., a damped substructure outrigger system (DSO). The novel system has good structural integrity due to its main structure consisting of the core tube, outrigger, and perimeter column. To present further investigation, the govern equations of DSO are derived by the simplified model which is regard as a cantilever beam system with a multirotation spring and energy dissipation substructure. Then, the energy distribution and seismic performance are parametric investigated. Finally, the damping effects of DSO are discussed. The results indicate that DSO possesses the superiority of damping performance. Compared with DO, DSO is less sensitive to perimeter column stiffness. Moreover, the proposed system can obtain the high efficiency in energy dissipation but with less damping cost than that of the viscous damper. Also, the larger stroke of the viscous damper can be found for DSO.

1. Introduction

In modern cities, tall buildings have vastly increased over the last decades, as they can contribute a high ratio floor space per area of land [1, 2]. Tall building is one of the urban symbols, and their structural safety is the primary requirement. Tall buildings typically consist of structural systems whose design is governed by the lateral loading cases [2]. To decrease the structural deformation induced by lateral loadings such as the wind or earthquake, an outrigger system is introduced to apply into the tall building and present a higher later lateral resistance capacity [3–5]. The implementation of this working mechanism comes from a special collaboration of each structural element. For instance, when the outrigger system is subjected to the lateral loadings, the core undergoes bending deformation, which leads to outriggers rotation. Interestingly, the rotation will be suppressed by allowing compression and tension of peripheral columns. Finally, this mechanism helps to improve the efficiency of the core system by simply introducing the exterior columns to aid in resisting part of the overturning moment caused by lateral loads [6–8]. It is thus clear that this excellent performance owe to the coupling of outriggers, core, and perimeter columns [9], which also make the outrigger system a suitable alternative for high-rise building constructions [10–14]. However, for this system, the huge inner force occurs in the connection position of outriggers and the core under an earthquake or wind exercitation, which may cause serious damage to the structure [7, 15]. Thus, the higher energy dissipation outrigger system becomes more and more attractive for tall buildings [16].

It is known that TMD (tuned mass damper) has been widely applied for the vibration control of tall buildings in the past decades [17]. Many research studies have confirmed that TMD is effective in wind vibration suppression. However, it should also be noted that its application in seismic reduction is open to further discussion. Fortunately, in recent years, a damped outrigger system (DO) is proposed to enhance the seismic performance, in which the links between outriggers and perimeter columns in traditional outrigger system (TO) have been artificially disconnected; meanwhile, the viscous dampers are implemented into the gaps [12, 18–20]. Such operation releases the force between the outriggers and perimeter columns and hence offers the large vertical relative deformation for damper energy dissipation, providing a significant damping effect for the whole structure [16, 21]. Moreover, the intrinsic damping of the traditional outriggers system has been effectively improved. In addition, the corresponding damping effects have also been verified with the results of real-time hybrid simulation [22, 23] and shaking table test [15]. At present, DO has been successfully applied in many practical projects [24–26].

To describe the dynamic behavior of the DO, theoretical simplified models, calculation methods, and experimental tests have been carried out [12, 14, 15, 18, 26–29]. To further achieve the best damping performance, the maximum damping ratio was adopted to obtain the optimal position of the outrigger and damping coefficient [12, 18]. Moreover, several multiobjective optimization processes were employed to reduce harmful interstory drift and other structural seismic responses [16, 30]. It should be noted that the relative motion between the outer end of the outrigger and the column may not be large enough to further enhance energy dissipation. Considering this limitation, Sun et al. [16, 31–33] introduced the negative stiffness devices into the outrigger system and obtained the better damping performance than the conventional damped outrigger. Moreover, being different from a tuned mass damper [34], frequency-independent damping is introduced to achieve the maximum value for damping ratios of all modes for the new system [35]. In addition, Liu et al. [36] proposed a novel energy dissipation outrigger system with a rotational inertia damper to increase the energy dissipation efficiency. However, above investigations heavily depend on the simplified model consisting of three critical components, i.e., the outriggers, the core tube, and perimeter columns. As shown in Figure 1, the direct connection between the outrigger and perimeter column of TO plays an important role in enhancing the total stiffness and maintaining the structural integrity. Nevertheless, dampers implemented in the gap between the outrigger and perimeter column of DO contribute to the more available deformation and enhance the damping efficiency. Meanwhile, this operation essentially disconnects the outrigger and column. Then, the composition consisted by the core tube and outriggers, and the perimeter columns are divided into two independent parts, in which perimeter columns has few contributions on the total stiffness. Therefore, the artificial disconnection of the outrigger and perimeter column for DO is essentially a potential threat for the structural safety. Fortunately, the buckling-restrained-brace outrigger system [37–39] is investigated as another type of dissipation outrigger system that has been widely applied and attaches more importance [9]. Also, there are a lot of creative measures, like toggle-brace, jack-scissor, gyro, and seesaw [40–43], in which they present well-controlled damping effects without losing the structural integrity for TO. However, these devices only make best of "one story" for energy dissipation, so that their work efficiencies are limited. Therefore, the structural integrity and damping efficiency of the outrigger system deserve the more researchers' attentions.

In fact, TO will force the perimeter column and central tube deform compatibly via outrigger with large stiffness, and thus significantly increases the stiffness and also guarantees the integrity of tall buildings. In this regard, TO can be assumed as tall buildings with mega components (i.e., main structure), where outrigger can be assumed to act as a mega-beam and the central core tube and perimeter column are mega-column. Thus, the structural integrity can be well-remained due to enough stiffness and loads resistance offered by the main structure. In addition, the substructure is located in two outriggers, in which its outer ends of the beams and columns of top floor are disconnected to main structure. Meanwhile, the dampers are replaced to the link between top floor of substructures and outriggers or core tube. As such, the proposed novel outrigger system is expected to obtain excellent performance. This is attributed to the larger relative deformation between the top substructure and the corresponding core or outrigger, so that the implemented damper can present powerful energy dissipation performance [44, 45]. At present, the structural integrity and damping efficiency of the outrigger system can be a trade-off for the proposed system.

Based on above, a new structural system is proposed by combining TO and damped substructures. The main structure presents enough stiffness and loads resistance, while the system is potential to obtain the higher efficiency in energy dissipation with less damping cost due to the amplification effect of concentrated interlayer deformation between top damped substructures and main structure. This study focuses on the seismic energy distribution and seismic performance of the novel structural system, which is divided into the following sections. First, the configuration of the proposed system is described, and then the govern equation of DSO are derived by the simplified model which is regard as a cantilever beam system with multirotation spring and energy dissipation substructure. Second, to explore the energy distribution and seismic performance, the random mean vibration energy and seismic response are parametric investigated. Finally, the damping effects of DSO and some suggestions for practical design are discussed.

2. Damped Substructure Outrigger (DSO) System

2.1. Formulation of the Proposed System. In this section, the detailed description of the construction process for DSO shown in Figure 2(a) is listed as follows. As shown in Figure 2(b), the main structure is similar to the mega-frame

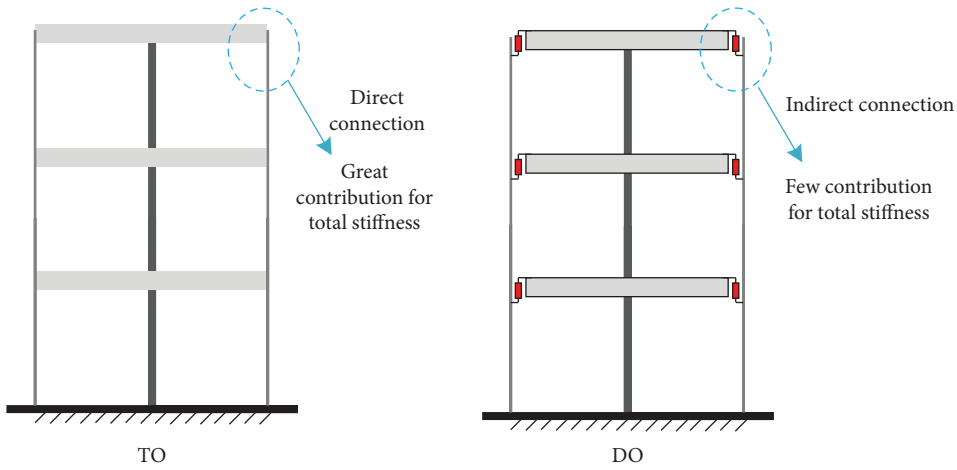

Figure 1: Comparison of TO and DO.

and consists of key components such as the outriggers, the core tube, and perimeter columns, so that the structural integrity can be well-remained due to enough stiffness and loads resistance offered by the main structure. In addition, the substructure is partly disconnected to the main structure, in which its outer ends of the beams and columns of top floor are separated from main structure. Thus, the top of substructure shown in Figure 2(c) is eventually the free end. Meanwhile, the dampers are arranged between top floor of substructures and the corresponding outriggers or core tube. As such, the larger relative deformation is concentrated the gap of top substructure and the corresponding core or outrigger, in which it is profit for the implemented dampers to achieve full potential energy dissipation. In other word, compared with the "one story" deformation, "multistory" deformation mechanism can be obtained to present the damping amplification. In addition, note that the huge gravity loads can be supported by the mega beams and the mega columns of mega substructure [44, 45]. Similarly, the huge gravity loads also can be supported by the outriggers, perimeter columns, and the core tube of the proposed outrigger system. Moreover, the core tube is designed in the center of the plan and thus the outrigger only withstands half moment of the mega beams of mega sub-structure. As such, it is feasible for the proposed outrigger system. However, the outriggers, perimeter columns, and the core tube should be strengthened to these of the tradition outrigger system.

There is a clear difference between the main structure of the DSO and mega-frame of the mega subcontrolled system. This is because the mega-frame is mainly shear deformation under lateral loadings, while the main structure of DSO shown in Figure 2(b) behaves bending deformation, and only the substructure shown in Figure 2(c) is shear deformation. In view of this, DSO is essentially simplified to be a cantilever beam system with multirotation spring and energy dissipation substructure (seen by Figure 2(d)). However, as the equivalent multi-rotation-springs made by the outriggers and columns may casus complex coupling behaviors, and the seismic analysis will be more difficult with consideration of substructures. As such, the dynamic characteristic of DSO is significantly different from the mega-sub controlled structure; hence, further investigation should be carried out to present the well-design suggestions.

2.2. Analytical Model of DSO. According to the above analysis, DSO can be described as a uniform cantilever beam (the core tube) system with a multirotation spring, in which each top floor of substructure and corresponding outrigger or the core tube is linked by a damper. Thus, the final simplified model is shown in Figure 2(d). For convenience, DSO with three outriggers is illustrated in this study, in which the bending stiffness of outriggers and the axial stiffness of perimeter columns are taken into account. The bending stiffness of outriggers is E_oI_o and the length of each outrigger, r, is scaled from its outer end to the centre of the core tube. The outrigger stiffness ratio is defined as $\gamma = 2EIr/(E_oI_oH)$. As shown in Figure 2(d), the core tube with bending stiffness EI is modeled as a cantilever beam and its length is H. In addition, the distance between the fixed end of the core and outrigger positions are, $\alpha_1 H$, $\alpha_2 H$, $\alpha_3 H$, $\ldots$, $\alpha_v H$, where v is the number of substructures. As for the perimeter columns, each segment can be viewed as a vertical spring, k_{e_j}. They can be calculated by $k_{e_1} = E_cA_c/(\alpha_1 H)$, $k_{e_j} = E_cA_c/(\alpha_j - \alpha_{j-1})H$, $j = 2, 3, \cdots, v$, where E_cA_c is the axial stiffness of the perimeter columns and the stiffness ratio can be expressed as $\beta = EI/(2r^2E_cA_c)$. $u_1, u_2, \cdots, u_v$ are vertical displacement of the outer end of outriggers. c_{d_j} is the damping coefficient of jth outrigger damper and f_{d_j} is the corresponding damping force. k_{θ_j} is the equivalent stiffness of resistance rotation spring which consists of outriggers and perimeter columns, and can be described as followings.

As the bending stiffness of outriggers and the axial stiffness of perimeter columns are taken into account in this paper, the axial deformation of perimeter column and bending deformation of outrigger should be considered. Figure 3 illustrates the process. The extra vertical deformation at outrigger end is Δ_u (Figure 3(a)), in which a spring with stiffness k_o attached at the outrigger end can be equivalent to outrigger's bending stiffness (Figure 3(b)), and the bending stiffness is regard as the infinite stiffness at the

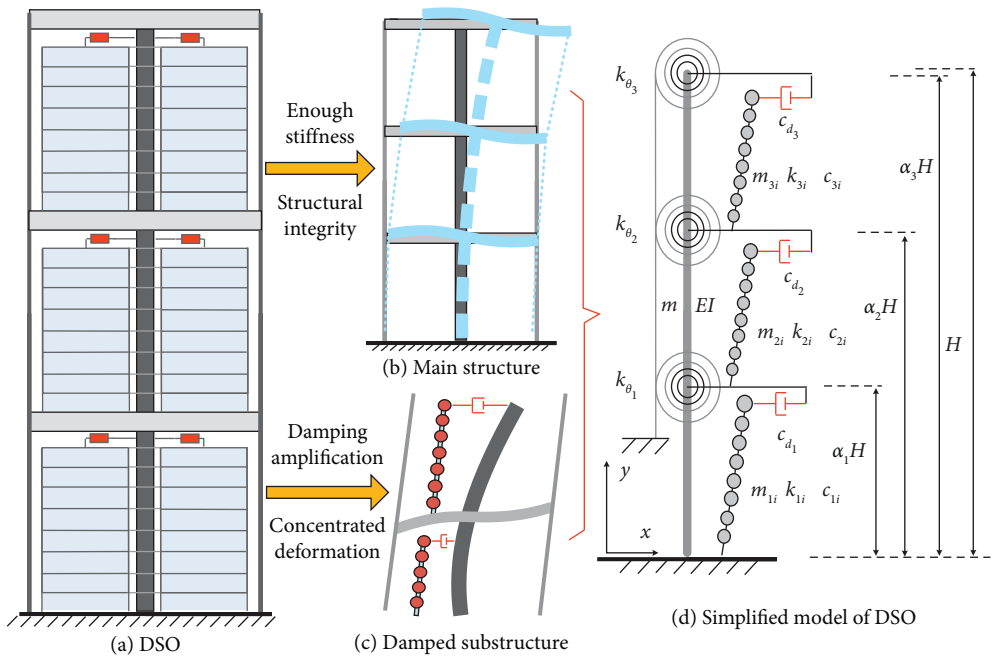

Figure 2: Structural composition and simplification.

same time. When considering the axial stiffness of the perimeter column, the force generated by the outrigger and perimeter column can be written as given in the following equation (Figure 3(d)):

$$\begin{aligned} F_k &= k_o\left(u' - u\right) \\ &= k_e u. \end{aligned} \tag{1}$$

The equivalent vertical spring of the outrigger is $k_o = 3E_oI_o/r^3$. As shown in Figure 3(a), the practical deformation u at the end of outrigger is

$$u = u' + \Delta_u, \tag{2}$$

where u' is the deformation only considering rigid body rotation of the outrigger. Equation (1) yields $u = k_o u'/(k_e + k_o)$. Combining equation (1) yields (see Figure 3(d)).

$$F_k = k_{eo} u', \tag{3}$$

where $k_{eo} = k_e k_o/(k_e + k_o)$ is the equivalent stiffness of the outrigger and perimeter column.

Hereafter, the equivalent model with infinitely stiff outrigger is adopted (Figure 3(d)), i.e., outrigger stiffness ratio γ is assigned as a small value [32].

2.3. Dynamic Equation of DSO. As described before, DSO is a complex structure system, and the dynamic equation derivation is also a tedious process. Thus, the basic derivation procedure of the dynamic equation is presented in Figure 4. First, the finite-element method is utilized to derive the governing equation for the core tube under ground motion, in which the influences of the outriggers, perimeter columns, and substructure are taken into account. Then, the motion equations of the substructure are obtained by the force and rotation moment balance. Finally, the whole structure dynamic expressions can be obtained by combining the dynamic equations of the substructure and main structure. The detailed procedure is as follows.

2.3.1. Main Structure. As for the main structure, the core tube can be modeled by a uniform cantilever beam. Thus, the finite-element method is utilized to derive the governing equation for the core tube under ground motion. Similar to Section 2.2, the coupling model of multiple outriggers and perimeter columns can be expressed as

$$\mathbf{F}_k = \mathbf{k}_{eo}\mathbf{u}', \tag{4}$$

where $\mathbf{F}_k = [f_{e_1}, f_{e_2}, \cdots, f_{e_{n_c}}]^T$ are the forces generated by the outriggers and perimeter columns, $\mathbf{u}'$ is the vertical deformation at the end of outrigger, $\mathbf{k}_{eo}$ is the equivalent stiffness matrix coupled by the outriggers and perimeter columns, and it can be written as

$$\mathbf{k}_{eo} = \mathbf{k}_e\left(\mathbf{k}_e + \mathbf{k}_o\right)^{-1}, \tag{5}$$

where $\mathbf{k}_e = \begin{bmatrix} k_{e_1} + k_{e_2} & -k_{e_2} & & \\ -k_{e_2} & k_{e_2} + k_{e_3} & \ddots & -k_{e_v} \\ & \ddots & -k_{e_v} & k_{e_v} \end{bmatrix}$ and

$\mathbf{k}_o = \begin{bmatrix} k_{o_1} & & & \\ & k_{o_2} & & \\ & & \ddots & \\ & & & k_{o_v} \end{bmatrix}$.

The displacement at the end of the outriggers is rewritten as

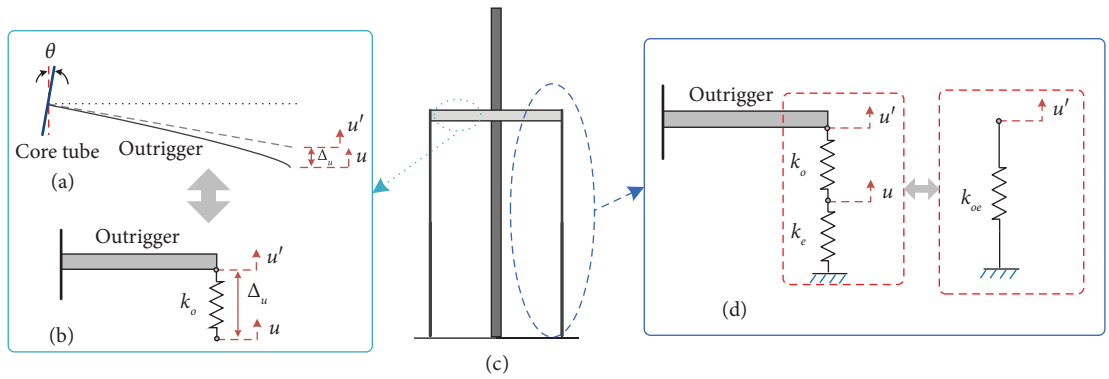

FIGURE 3: Structural simplification: (a) real deformation of outrigger; (b) equivalent model for outrigger; (c) original model; (d) equivalent model for outrigger with perimeter column.

$$\mathbf{u}' = r\boldsymbol{\theta}_c = r\left[\theta_1, \theta_2, \cdots, \theta_v\right]^T_{1\times v}, \tag{6}$$

where $\boldsymbol{\theta}_c$ is the rotation angle vector of all outriggers.

Assuming that the core tube is modeled with n_φ beam elements, the displacement vector containing nodes $1, 2, \cdots, n_\varphi$ can be listed as

$$\mathbf{u}_c = \left[u_{c_1}, \theta_{c_1}, u_{c_2}, \theta_{c_2}, \cdots, u_{c_{n_\varphi}}, \theta_{c_{n_\varphi}}\right]^T_{1\times 2n_\varphi}. \tag{7}$$

According to equation (7), assume $\boldsymbol{\theta}_c = \Gamma_\theta \mathbf{u}_c$, equation (6) can be rewritten as

$$\mathbf{u}' = r\Gamma_\theta \mathbf{u}_c, \tag{8}$$

where $\Gamma_\theta = [\Gamma_{\theta_1}; \Gamma_{\theta_2}; \cdots; \Gamma_{\theta_v}]_{v\times 2n_\varphi}$, $\Gamma_{\theta_j} = [0, 0, \cdots, 1, \cdots, 0]_{1\times 2n_\varphi}$, $\Gamma_{\theta_j}(2n_j) = 1$, and n_j represent n_jth beam element linked by jth outrigger. The force generated by equivalent spring is

$$\mathbf{F}_k = \mathbf{k}_{eo}\mathbf{u}'. \tag{9}$$

The resistant moments caused by the outriggers and perimeter columns are

$$\mathbf{M}_\theta = -2r\mathbf{F}_k, \tag{10}$$

where $\mathbf{M}_\theta = [\mathbf{M}_{\theta_1}, \mathbf{M}_{\theta_2}, \cdots, \mathbf{M}_{\theta_v}]$. Substituting equation (8) into equations (9) and (10), yields the following equation:

$$\mathbf{M}_\theta = -2r^2\mathbf{k}_{eo}\Gamma_\theta \mathbf{u}_c = \mathbf{k}_\theta \boldsymbol{\theta}_c, \tag{11}$$

where $\mathbf{k}_\theta = -2r^2\mathbf{k}_{eo}$ is the matrix of equivalent resistance rotation spring. The additional node force of jth outrigger is written as

$$\mathbf{F}_{\theta_j} = \begin{bmatrix} 0 & 0 & 0 & M_{\theta_j} \end{bmatrix}^T. \tag{12}$$

Let $\mathbf{M}_\theta$ add to the beam element, yields the equivalent node forces

$$\begin{aligned} \mathbf{F}_{\theta k} &= \Gamma_\theta^T \mathbf{M}_\theta \\ &= -2r^2\Gamma_\theta^T \mathbf{k}_{\text{eo}}\Gamma_\theta \mathbf{u}_c. \end{aligned} \tag{13}$$

Thus, the vibration equation of motion for the main structure is given by the following equation:

$$\mathbf{M}_z\ddot{\mathbf{u}}_c + \mathbf{C}_z\dot{\mathbf{u}}_c + \mathbf{K}_z\mathbf{u}_c - \mathbf{F}_{\theta k} = \mathbf{F}_g - \mathbf{f}_d\Gamma_\theta + \mathbf{M}_I\Gamma_s + \mathbf{f}_k\Gamma_s, \tag{14}$$

where $\mathbf{M}_z$, $\mathbf{C}_z$, and $\mathbf{K}_z$ are the mass matrix, damping matrix and stiffness matrix of the core tube. $\mathbf{F}_g$ is the inertial force caused by earthquake for the core tube and consists of $\mathbf{F}_{e_g} = -m\ddot{u}_g L/12\begin{bmatrix} 6 & L & 6 & -L \end{bmatrix}^T$ at each beam element. $\mathbf{f}_d = \begin{bmatrix} f_{d_1} & f_{d_2} & \cdots & f_{d_v} \end{bmatrix}_{1\times v}$ is the damping force. $\Gamma_s = [\Gamma_{\theta_2}; \Gamma_{\theta_3}; \cdots; \Gamma_{\theta_v}]_{(v-1)\times 2n_\varphi}$. $\mathbf{M}_I$ is the inertia moment which has the form of $\mathbf{M}_I = \begin{bmatrix} M_{I_1} & M_{I_2} & \cdots & M_{I_v} \end{bmatrix}_{1\times v}$, in which M_{I_j} can be expressed as

$$M_{I_j} = -\sum_{i=1}^{n} m_{ji}\left(\ddot{x}_g + \ddot{x}_{s_{ji}} + \ddot{x}_{b_{j-1}} - \ddot{\theta}_{b_{j-1}}h_{s_{ji}}\right)h_{s_{ji}} + f_{d_j}h_{s_{jn}}, \tag{15}$$

where $j > 1$. $\mathbf{f}_k$ is the base force of the substructure and can be expressed as $\mathbf{f}_k = \begin{bmatrix} f_{k_2} & f_{k_3} & \cdots & f_{k_v} \end{bmatrix}_{1\times v}$. f_{k_j} has the form of

$$f_{k_j} = -\sum_{i=1}^{n} m_{ji}\left(\ddot{x}_g + \ddot{x}_{s_{ji}} + \ddot{x}_{b_{j-1}} - \ddot{\theta}_{b_{j-1}}h_{s_{ji}}\right)h_{s_{ji}} + f_{d_j}. \tag{16}$$

2.3.2. Substructure. In fact, the outrigger rotation in practical outrigger system is an important factor for substructures and then affects structural dynamic characteristic. Therefore, the rotation effect of the outrigger is also considered for the substructure. To explain the rotational influence on substructure, the simplified model of the $(j+1)$th substructure shown in Figure 5 is adopted to describe the dynamic behavior. The various parameters are defined as followings. $x_{s_{j+1,i}}$ is ith floor displacement of the $(j+1)$th substructure relative to jth outrigger. x_g is the displacement of the ground. x_{b_j} is the displacement of jth outrigger relative to ground. $\theta_j h_{j+1,i}$ is the displacement caused by the rotation of outrigger, in which θ_j is the rotation angle of the jth

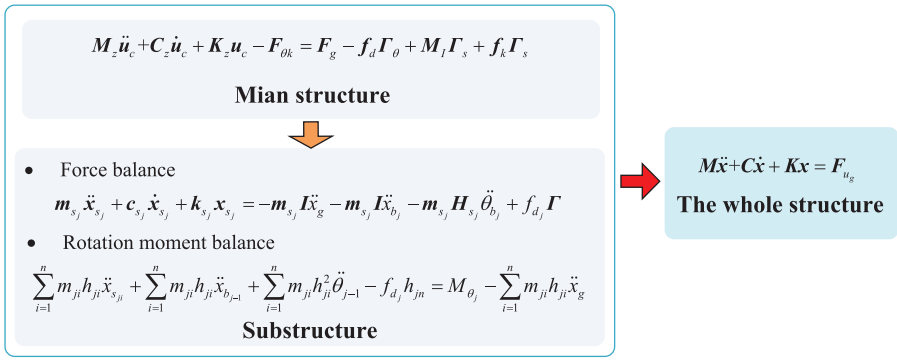

Figure 4: The basic derivation procedure of the dynamic equation.

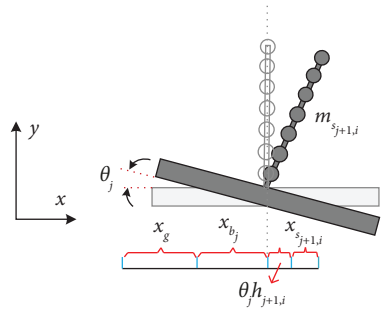

Figure 5: $(j+1)$th substructure.

outrigger and $h_{j+1,i}$ is the ith floor height of the $(j+1)$th substructure.

The first substructure $(j=1)$ is a partly independent system because only its base directly links to the ground (see Figure 2(d)). The motion equation is written as

$$\mathbf{m}_{s_1}\ddot{\mathbf{x}}_{s_1} + \mathbf{c}_{s_1}\dot{\mathbf{x}}_{s_1} + \mathbf{k}_{s_1}\mathbf{x}_{s_1} = -\mathbf{m}_{s_1}\mathbf{I}\ddot{x}_g + f_{d_1}\Gamma, \tag{17}$$

where $\Gamma = [0, \cdots, 0, 1]^T_{1\times n}$, n is floor number of the substructure. $\mathbf{x}_{s_1} = [x_{11}, x_{12}, \cdots, x_{1n}]^T_{1\times n}$ is the displacement vector of substructure, $f_{d_1} = c_{d_1}(\dot{x}_{b_1} - \dot{x}_{s_{1n}})$ is the damping force vector generated by damper installed between top of substructure and corresponding the core tube.

If $j>1$, the vibration equation of jth substructure is expressed as

$$\begin{aligned}\mathbf{m}_{s_j}\ddot{\mathbf{x}}_{s_j} + \mathbf{c}_{s_j}\dot{\mathbf{x}}_{s_j} + \mathbf{k}_{s_j}\mathbf{x}_{s_j} = &-\mathbf{m}_{s_j}\mathbf{I}\ddot{x}_g - \mathbf{m}_{s_j}\mathbf{I}\ddot{x}_{b_j} \\ &- \mathbf{m}_{s_j}\mathbf{H}_{s_j}\ddot{\theta}_{b_j} + f_{d_j}\Gamma,\end{aligned} \tag{18}$$

where $\mathbf{x}_{s_j} = [x_{j1}, x_{j2}, \cdots, x_{jn}]^T_{1\times n}$, $f_{d_j} = c_{d_j}(\dot{x}_{b_j} - \dot{x}_{s_{jn}} - \dot{x}_{b_{j-1}} - \dot{\theta}_{b_{j-1}}h_{s_{jn}})$, $\mathbf{H}_{s_j} = [h_{s_{j1}}, h_{s_{j2}}, \cdots, h_{s_{jn}}]^T_{1\times n}$,

$$\mathbf{m}_{s_j} = \begin{bmatrix} m_{s_{j1}} & & & \\ & m_{s_{j1}} & & \\ & & \ddots & \\ & & & m_{s_{jn}} \end{bmatrix}_{n\times n},$$

$$\mathbf{k}_{s_j} = \begin{bmatrix} k_{s_{j1}} & -k_{s_{j2}} & & \\ -k_{s_{j2}} & k_{s_{j2}} + k_{s_{j3}} & \ddots & -k_{s_{jn}} \\ & & & k_{s_{jn}} \\ & -k_{s_{jn}} & & \end{bmatrix}_{n\times n},$$

and

$$\mathbf{c}_{s_j} = \begin{bmatrix} c_{s_{j1}} & -c_{s_{j2}} & & \\ -c_{s_{j2}} & c_{s_{j2}} + c_{s_{j3}} & \ddots & -c_{s_{jn}} \\ & & -c_{s_{jn}} & c_{s_{jn}} \end{bmatrix}_{n\times n}$$

Based on the rotation moment balance, jth $(j>1)$ substructure can be expressed as

$$\begin{aligned}&\sum_{i=1}^{n} m_{ji}h_{ji}\ddot{x}_{s_{ji}} + \sum_{i=1}^{n} m_{ji}h_{ji}\ddot{x}_{b_{j-1}} + \sum_{i=1}^{n} m_{ji}h_{ji}^2\ddot{\theta}_{j-1} - f_{d_j}h_{jn} \\ &\quad = M_{\theta_j} - \sum_{i=1}^{n} m_{ji}h_{ji}x_g,\end{aligned} \tag{19}$$

where M_{θ_j} is the jth outrigger resistant moment generated by the core tube.

2.3.3. The Whole Structure. With the dynamic equation of the substructure and main structure, the whole structure expressions can be easily obtained. Combine the equations (14), (18), and (19), yields the total dynamic equation

$$\mathbf{M}\ddot{\mathbf{x}} + \mathbf{C}\dot{\mathbf{x}} + \mathbf{K}\mathbf{x} = \mathbf{F}_{u_g}, \tag{20}$$

where $\mathbf{M}$, $\mathbf{C}$, and $\mathbf{K}$ are the total mass matrix, damping matrix, and stiffness matrix, respectively. They can be expressed as following forms. The total mass matrix is written as

$$\mathbf{M} = \begin{bmatrix} \mathbf{M}_{11} & & & & \\ \mathbf{0} & \mathbf{M}_{22} & & sym & \\ \mathbf{M}_{31} & \mathbf{0} & \mathbf{M}_{33} & & \\ \vdots & \vdots & \vdots & \ddots & \\ \mathbf{M}_{v+1,1} & \mathbf{0} & \mathbf{0} & \mathbf{0} & \mathbf{M}_{v+1,v+1} \end{bmatrix}_{(2n_\varphi+nv)\times(2n_\varphi+nv)}, \quad (21)$$

where $\mathbf{M}_{11} = \mathbf{M}_z + \mathbf{M}_{zs}$, $\mathbf{M}_{zs}(2n_j-1:2n_j, 2n_j-1:2n_j) = \begin{bmatrix} \sum_{i=1}^{n} m_{ji} & \sum_{i=1}^{n} m_{ji}h_{ji} \\ \sum_{i=1}^{n} m_{ji}h_{ji} & \sum_{i=1}^{n_c} m_{ji}h_{ji}^2 \end{bmatrix}$, and other elements are 0. n_j is the n_jth beam element which is linked to the base of jth outrigger. $\mathbf{M}_{j+1,j+1} = \mathbf{m}_{s_j}$. $\mathbf{M}_{j+1,1}(1:n, 1:2) = \begin{bmatrix} m_{j1} & m_{j1}h_{j1} \\ m_{j2} & m_{j2}h_{j2} \\ \vdots & \vdots \\ m_{jn} & m_{jn}h_{jn} \end{bmatrix}_{n\times 2}$ and other elements are 0, $j > 1$.

The total stiff matrix is written as

$$\mathbf{K} = \begin{bmatrix} \mathbf{K}_z + 2r^2\Gamma_\theta \mathbf{k}_{eo}\Gamma_\theta^T & & & & \\ & \mathbf{k}_{s_1} & & & \\ & & \mathbf{k}_{s_2} & & \\ & & & \ddots & \\ & & & & \mathbf{k}_{s_v} \end{bmatrix}_{(2n_\varphi+nv)\times(2n_\varphi+nv)}. \quad (22)$$

The total damping matrix is written as

$$\mathbf{C} = \mathbf{C}_{z0} + \mathbf{C}_{zs},$$
$$\mathbf{C}_{z0} = \begin{bmatrix} \mathbf{C}_{zc} & \mathbf{0} & \mathbf{0} & \cdots & \mathbf{0} \\ \mathbf{0} & \mathbf{0} & \mathbf{0} & \cdots & \mathbf{0} \\ \mathbf{0} & \mathbf{0} & \mathbf{0} & \cdots & \mathbf{0} \\ & \vdots & \vdots & \vdots & \ddots \ \mathbf{0} \\ \mathbf{0} & \mathbf{0} & \mathbf{0} & \mathbf{0} & \mathbf{0} \end{bmatrix}_{(2n_\varphi+nv)\times(2n_\varphi+nv)}, \quad (23)$$

where $\mathbf{C}_{zc} = (\phi^T)^{-1}\mathbf{C}^*\phi^{-1}$ is the damping matrix outrigger system with substructure but no dampers implemented, ϕ is the corresponding mode matrix. $\mathbf{C}^*$ is the damping coefficient matrix, and it is a diagonal matrix which consists of $C_i = 2M_i\omega_i\xi_i, i = 1, 2, \cdots, n_\omega$. C_i is ith modal damping coefficient, M_i is ith modal mass, ω_i is ith modal frequency, ξ_i is ith modal damping ratio, n_ω is the number of modal order. For convenience, each damping ratio is assumed as the same value.

$$\mathbf{C}_{zs} = \begin{bmatrix} \mathbf{C}_{11} & & & & \\ \mathbf{C}_{21} & \mathbf{C}_{22} & & sym & \\ \mathbf{C}_{31} & \mathbf{0} & \mathbf{C}_{33} & & \\ \vdots & \vdots & \vdots & \ddots & \\ \mathbf{C}_{v+1,1} & \mathbf{0} & \mathbf{0} & \mathbf{0} & \mathbf{C}_{v+1,v+1} \end{bmatrix}_{(2n_\varphi+nv)\times(2n_\varphi+nv)}, \quad (24)$$

where $\mathbf{C}_{11}$ is the damping matrix $2n_\varphi \times 2n_\varphi$ which has the same size of $\mathbf{C}_{zc}$. $\mathbf{C}_{11}(2n_j-1:2n_j, 2n_j-1:2n_j) = \begin{bmatrix} c_{d_j}+c_{d_{j+1}} & c_{d_{j+1}}h_{jn} \\ c_{d_{j+1}}h_{jn} & c_{d_{j+1}}h_{jn}^2 \end{bmatrix}$, $j = 1, 2, v-1$; If $j = v$, it can be $\mathbf{C}_{11}(2n_v-1:2n_v, 2n_v-1:2n_v) = \begin{bmatrix} c_{d_v} & 0 \\ 0 & 0 \end{bmatrix}$; $\mathbf{C}_{11}(2n_j, 2n_j-1:2n_j) = \begin{bmatrix} -c_{d_j} & -c_{d_j}h_{jn} \end{bmatrix}$; $\mathbf{C}_{11}(2n_j-1: 2n_j, 2n_j) = \mathbf{C}_{11}^T(2n_j, 2n_j-1:2n_j)$, $j = 1, 2, v-1$, $\mathbf{C}_{j+1,j+1} = \begin{bmatrix} 0 & \cdots & \\ \vdots & \ddots & \text{sym} \\ 0 & \cdots & 0 \ 0 \\ 0 & \cdots & 0 \ c_{d_j} \end{bmatrix}_{n\times n}$, $j = 1, 2, \ldots, v$.

When $j = 1$, $\mathbf{C}_{21}(n, 2n_1-1) = -c_{d_1}$, in which $\mathbf{C}_{21}$ has the size of $n \times 2n_\varphi$ and other elements are 0. Similarly, $j > 1$, $\mathbf{C}_{j+1,1}$ has the size of $n \times 2n_\varphi$, in which $\mathbf{C}_{j+1,1}(n, 2n_{j-1}-1:2n_{j-1}) = [c_{d_j}\, c_{d_j}h_{jn}]$, $\mathbf{C}_{j+1,1}(n, 2n_j-1) = -c_{d_j}$ and other elements are 0. $\mathbf{F}_{u_g}$ is the total inertial force vector caused by ground motion and can be expressed as

$$\mathbf{F}_{u_g} = -\ddot{x}_g \begin{bmatrix} \mathbf{F}_g + \mathbf{F}_s \\ \mathbf{F}_1 \\ \mathbf{F}_1 \\ \vdots \\ \mathbf{F}_v \end{bmatrix}_{(2n_\varphi+nv)\times 1}, \quad (25)$$

where $\mathbf{F}_s(2n_{j-1}-1:2n_{j-1}) = \begin{bmatrix} \sum_{i=1}^{n} m_{ji} & \sum_{i=1}^{n} m_{ji}h_{ji} \end{bmatrix}^T$ and $\mathbf{F}_j = \mathbf{m}_{s_j}\mathbf{I}$ are the contribution of the substructure.

3. The Vibration Energy Distribution and Parametric Study

In this study, an outrigger system with the height of $H = 210$ m is illustrated to present the seismic performance analysis, in which $\alpha = 1/3$, $\alpha = 2/3$ and $\alpha = 1$ of the core tube are taken as the position for three outriggers. The inherent damping is assumed to be 2% for each mode. Besides, the moment of inertia and the concrete elasticity modulus of the core tube are $I = 600\,\text{m}^4$ and $E = 3.6 \times 10^{10}$ Pa, respectively. The distributed mass along the height, $m = 120000$ kg/m (the mass distribution including main structure and substructures, and the total mass is $m^* = mH$). The outer end of outrigger to the center of the core, $r = 12$ m. The outrigger stiffness ratio is presented by $\gamma = 0.01$ to give the convenience for further investigation, in which the equivalent processes are listed in Section 2.2. Note that TO, DO, and DSO have the same building information as above mentioned, while each substructure for DSO is assumed the same number of floors ($n = 14$) and the same storey height $h = 5$ m. To give the damping performance analysis under random excitation, the Kanai-Tajimi filtered white noise model is employed to simulate the input ground motion, in which bedrock spectral density is $S_0 = 4.65 \times 10^{-4}\,\text{m}^2/\text{s}^3$ and filtering parameters are $\omega_g = 15$rad/s and $\xi_g = 0.6$ [46], respectively.

DSO is a special and complex structure, in which any single indicator of seismic responses for main structure and

substructure may not present comprehensive description. Fortunately, energy is a comprehensive index for structural dynamic analysis. The structural energy represents the safety of the structure under seismic exercitation. Besides, it also can reveal the damping mechanism for the control system. Therefore, the vibration energy is a well-suited index for seismic performance of DSO and the corresponding energy distribution characteristic is corrected factor to damping performance. Generally, the random vibration energy can be expressed as twice the mean kinetic energy [47, 48], i.e., $E = \sum \widetilde{m}(\widetilde{v}^2)$, in which $\widetilde{m}$ is the mass or moment of inertia, $\widetilde{v}^2$ is the corresponding velocity variance or rotation velocity variance. Therefore, in this study, random vibration energy is employed to explore the seismic performance of DSO.

In addition, to provide better description for parametric study for DSO, f_s is defined as the first mode frequency ratio between substructure and main structure; mass ratio μ is defined as the total mass of all substructures over main structure; $\lambda = c_d/m^*$ is defined as the damping parameter and each damper damping coefficient is assumed as the same value, i.e., $c_d = c_{d_1} = \cdots = c_{d_v}$. Similarly, each of damper for DO is $c_b = c_{b_1} = \cdots = c_{b_v}$. However, the damper layouts shown in Figure 6 for simplified models of DO and DSO are different. For example, each outrigger of DO has two dampers linked by its end, while only one damper located nearby the outrigger of DSO. In other word, if three outriggers are adopted for DO and DSO, and then six dampers and three dampers are arranged for them, respectively.

3.1. Stiffness Ratio and Damping Parameter Influence. Figure 7 presents the total vibration energy over λ and β with $\mu = 1$, $f_s = 1$. In Figure 7, it is seen that DSO shows well-controlled performance in total vibration energy reduction, in which a lot of energy have been dissipated. Interestingly, the perimeter column stiffness ratio β behaves significant impact on vibration energy. For instance, the curve of $\beta = 0.1$ presents the least vibration energy both for TO and DSO, whereas that of $\beta = 2$ can obtain the largest energy reduction for DSO to TO. It is thus clear that $\beta = 0.1$ (larger stiffness of perimeter column) is profit for the structural safety of DSO and TO. Most importantly, DSO still can remain the excellent control effects even the small stiffness of perimeter column (e.g., $\beta = 2$) is selected. For example, the vibration energy of DSO has a reduction of 71.05% to that of TO when $\beta = 2$ and $\lambda = 1.01$. However, note that small stiffness of the perimeter column will seriously deteriorate the damping performance of the DO [12, 49]. Fortunately, DSO can contribute the stable damping performance.

In addition, the vibration energy is also sensitive to the damping parameters, in which the energy first decreases with the λ rising, and then increases. In other words, there is an optimal value for the damping parameter, in which the vibration energy remains in the valley. More importantly, it can be seen from Figure 7 that the smaller value of β commonly needs a larger value of optimal λ to achieve better performance (e.g., $\lambda_{\text{opt}} = 0.17$, $\lambda_{\text{opt}} = 0.23$ and $\lambda_{\text{opt}} = 0.37$ when $\beta = 2$, $\beta = 0.5$ and $\beta = 0.1$). Then, the corresponding energy curve trends to be flat as $\lambda > \lambda_{\text{opt}}$, i.e., $\lambda > \lambda_{\text{opt}}$ is less impact on the damping performance for DSO.

Total vibration energy is the critical index of DSO, while the energy distribution of different structural components significantly influences its seismic performance. As shown in Figure 8, the vibration energy distribution of DSO is presented, in which the proportion represents the vibration energy ratio of the substructure or main structure over the whole vibration energy. Also, the red solid line and blue dotted line in Figure 8 represent the vibration energy and energy proportion for each part, respectively. Generally, for the vibration energy, the main structure and three substructures show the same change laws. For example, they have optimal damping parameters which locates in range of 0-1 for λ. Besides, the smaller β trends to obtain the larger optimal λ and leads to lower total vibration energy shown in Figure 7, such as $E_k = 8.49 \times 10^4$ J with $\beta = 0.1$ and $\lambda_{\text{opt}} = 0.17$. However, the vibration energy proportions of both the main structure and substructure shown in Figure 8 perform various changes when compared to those of energy distribution.

As seen in Figure 8(a), when $\lambda < 1$, the energy ratio of the main structure increases rapidly with the increase of λ. However, the energy ratio curves of the substructures basically display the downtrend shown in Figures 8(c) and 8(d). Moreover, the stiffness ratio β of the perimeter column shows less impact on the energy ratio except the 2nd substructure. When $\lambda > 1$, there is no evidently change for the energy proportion of the main structure and the curves gradually tends to be stable value of 0.4. Moreover, the proportion will be larger when the smaller stiffness ratio β of the perimeter column is adopted. Meanwhile, the cases of the substructure shown in Figures 8(b)–8(d) are relatively complex. For example, the 1st and 2nd substructures present the same change trend, in which the energy ratios increase with increase of λ. The 3rd substructure shows a downtrend, but its proportion is still close to 0.4. In general, when $\lambda < 1$, more energy transfers to the substructures and the energy proportion even larger than 0.7. When $\lambda > 1$ more energy focuses main structure (mainly for the core tube) and the energy proportion is close to 0.4. Interestingly, the minimum total vibration energy (Figure 7) is located in the range of λ for 0–0.5, whereas the main structure and substructures are also obtain the smaller vibration energy (Figure 8). Moreover, when λ_{opt} is selected, the energy ratio of main structure is close to 0.3 shown in Figure 8(a) and that of all substructures is close to 0.7 shown in Figures 8(b)–8(d). Therefore, it can be seen that the main structure not only has the lower energy but also locates in a lower energy proportion range. The above results indicate that main structure can keep in a relatively safe state and the substructure is easier to break first. This mechanism is actually critical to structural safety performance.

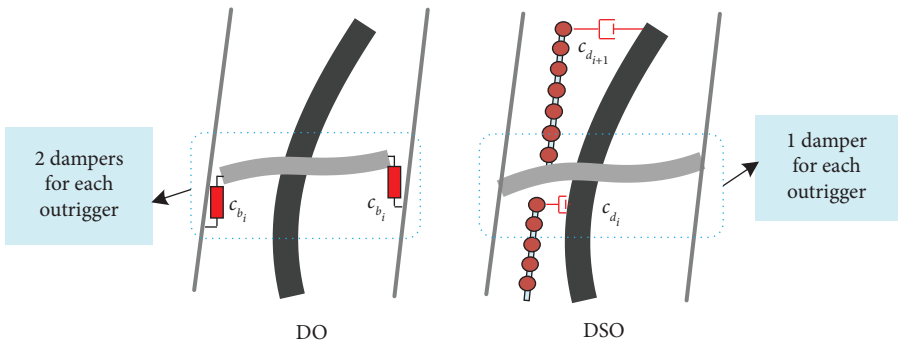

Figure 6: Dampers arranged for simplified model of DO and DSO.

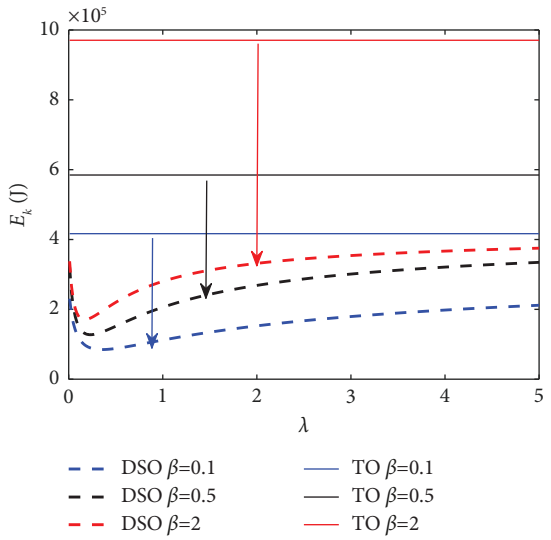

Figure 7: The total vibration energy versus λ and β ($\mu = 1, f_s = 1$).

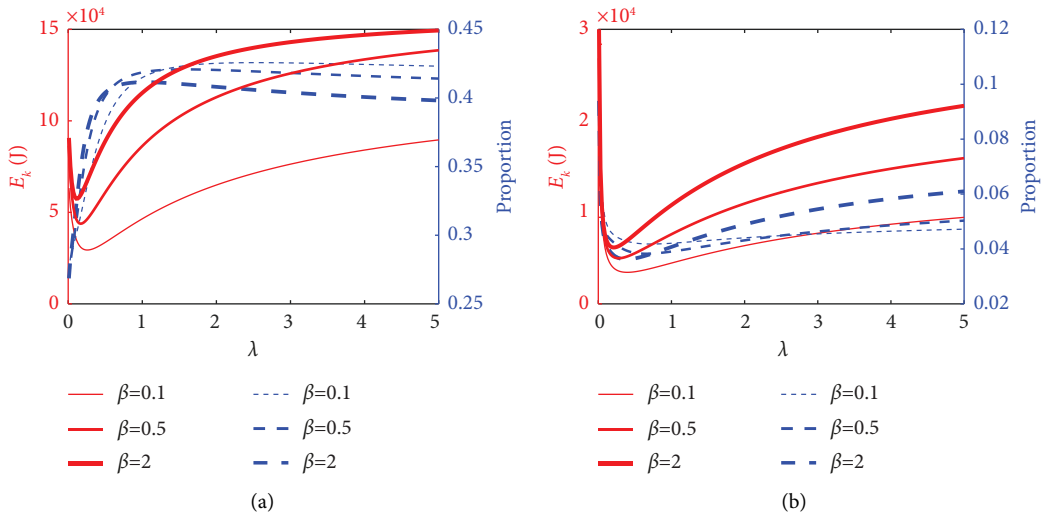

Figure 8: Continued.

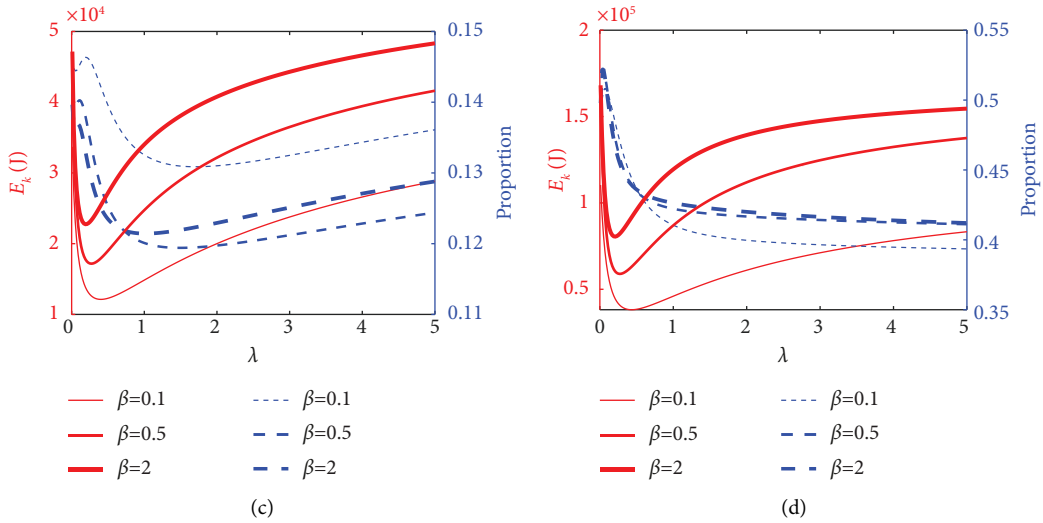

FIGURE 8: The vibration energy distribution for each part of DSO ($\mu = 1, f_s = 1$). (a) Main structure. (b) 1st substructure. (c) 2nd substructure. (d) 3rd substructure.

3.2. Frequency Ratio and Damping Parameter Influence. Figure 9 shows the total vibration energy over λ and f_s with $u = 1, \beta = 0.5$. When compared to the TO, less vibration energy can be observed in DSO. Moreover, the frequency ratio f_s significantly affects the total vibration energy, in which $f_s = 0.5$ (blue dotted line) contributes the least energy $E_k = 7.27 \times 10^4$ J when $\lambda = \lambda_{\text{opt}}$ is adopted. Interestingly, $f_s = 2.5$ (red dotted line) obtains the largest energy $E_k = 1.52 \times 10^5$ J with $\lambda = \lambda_{\text{opt}}$, but when $\lambda > 0.7$, its vibration energy is always at the lowest value compared with those of $f_s = 1$ and $f_s = 0.5$. Generally, f_s behaves sensitively to vibration energy. The above results also indicate that smaller f_s can obtain the minimum vibration energy, but the total vibration energy is more sensitive to λ.

To present further parameters investigation, the vibration energy distribution for each part of DSO with $u = 1, \beta = 0.5$ is shown in Figure 10. It can be seen in Figure 10 that frequency ratio f_s also significantly affects the vibration energy of main structure and substructure. The basic regularities of the vibration energy curves concluded by the Figure 10 are similar to those of Figure 9. However, the 1st substructure shows the opposite point shown in Figure 10(b), i.e., $f_s = 2.5$ obtains the lowest vibration energy for 1st substructure. Interestingly, the distribution proportion of vibration energy for the main structure increases rapidly with the increase of $\lambda < 0.5$ and trends to be plain with $\lambda > 0.5$ shown in Figure 10(a). Moreover, various f_s shows much different in vibration energy, and the larger f_s results in more energy focus in main structure. For instance, the energy proportion of $f_s = 0.5$ trends to be 0.28, that of $f_s = 1$ trends to be 0.42 and that of $f_s = 2.5$ trends to be 0.47. It is thus clear that the lower value of f_s is better for the main structure safety. In other words, the more vibration energy will transfers from the main structure to substructures. As for energy of the substructures shown in Figures 10(b)–10(d), they display the relatively complex cases. For example, the energy ratios of 1st and 2nd substructures are contrary to that of main structure, while the 3rd substructure has no obvious regularity for f_s except the $\lambda > 1$. Furthermore, $f_s = 2.5$ almost contributes a lower energy ratio for each substructure. Besides, the upper substructure commonly obtains the larger vibration energy ratio, i.e., the more vibration energy is transferred to it such as in the 3rd substructure. In general, based on λ_{opt}, the smaller of f_s results in a lower total vibration energy and vibration energy ratio of the main structure.

3.3. The Optimal Damping Parameter and the Corresponding Total Vibration Energy. Figure 11 shows the optimal damping parameter c_{opt} and the corresponding total vibration energy versus β and f_s, in which c_{opt} represents $c_{b_{\text{opt}}}$ (DO) or $c_{d_{\text{opt}}}$ (DSO). As seen in Figure 11, DO is employed to presents comprehensive comparison and $c_{b_{\text{opt}}}$ is the optimal damping coefficient of the damper linked by top of substructure and corresponding outrigger. As for the DSO, $c_{d_{\text{opt}}}$ can be achieved by the simple translation of λ_{opt}, i.e., $\lambda_{\text{opt}} = c_{d_{\text{opt}}}/(m^*)$. Optimal results shown in Figure 11(a) indicate that c_{opt} for both the DO and DSO decreases with β increasing. However, DSO is far less damping cost than DO, and the lower f_s leads to less damping cost. In addition, it can be seen by Figure 11(b) that the lower total vibration energy of DO can be obtained, particularly $\beta < 1.2$. However, DSO has the larger vibration energy. Fortunately, this case can be improved with the smaller f_s, such as $f_s = 0.5$, and it even outperforms the DO when $\beta > 1.2$. Thus, DSO can still achieve the well-controlled performance and substantially saves larger damping cost. For example, when $\beta = 2.1$, the total vibration energy of DO is $E_k = 1.28 \times 10^5$ J, while these of DSO are $E_k = 9.75 \times 10^4$ J, $E_k = 1.71 \times 10^5$ J and $E_k = 2.23 \times 10^5$ J for $f_s = 0.5$, $f_s = 1$ and $f_s = 2.5$, respectively. Most importantly, compared to the optimal damping coefficient $c_{b_{\text{opt}}} = 8.09 \times 10^7$ N·s/m for DO ($2c_{b_{\text{opt}}} = 1.18 \times 10^8$ N·s/m for each outrigger), these of DSO are $c_{d_{\text{opt}}} = 1.76 \times 10^6$ N·s/m, $c_{d_{\text{opt}}} = 4.28 \times 10^6$ N·s/m and

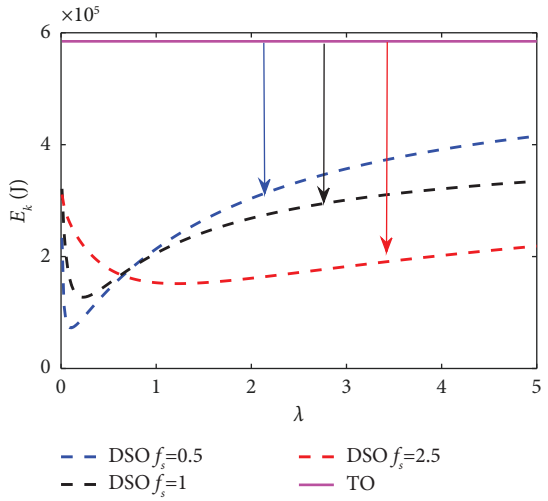

FIGURE 9: The total vibration energy versus λ and f_s ($u = 1, \beta = 0.5$).

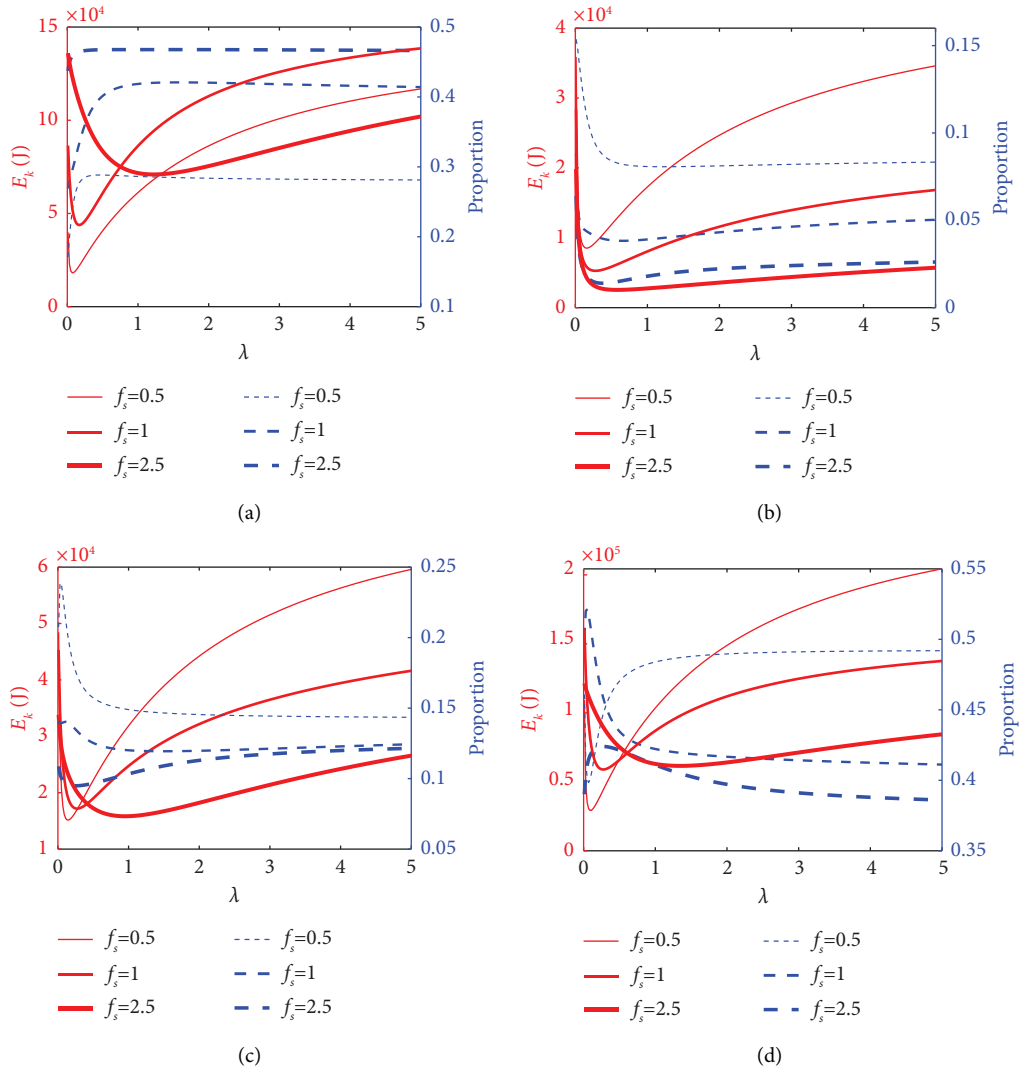

FIGURE 10: The vibration energy distribution for each part of DSO ($u = 1, \beta = 0.5$). (a) Main structure. (b) 1st substructure. (c) 2nd substructure. (d) 3rd substructure.

$c_{d_{opt}} = 2.34 \times 10^7$ N·s/m for $f_s = 0.5$, $f_s = 1$ and $f_s = 2.5$, respectively. Therefore, as mentioned above, DSO is greatly potential in seismic reduction and save the damping cost.

4. Seismic Performance Analysis

Seismic performance analysis will be conducted in time-history. The main building information has been listed in Section 3. As the fundamental frequency of the substructure is generally larger than that of the main structure; and hence, $f_s = 2.5$ is selected. In addition, based on the consideration that the total mass of substructures is close or larger than that of main structure; and hence, the mass ratio $u = 1$ is employed in this study. Then, the fundamental frequency of main structure is 1.83 rad/s and that of DSO without damper is 1.28 rad/s. With the above parameters, the time-history responses and energy comparison under the El Centro and Northridge ground motion records are presented, in which the acceleration amplitudes are uniformly adjusted to 0.4 g. Then, the results are shown in the following sections.

4.1. Structural Responses under Earthquake. Figures 12 and 13 show the structural responses under El Centro and Northridge earthquakes, in which Figures 12(a)–12(c) and 13(a)–13(c) are the floor displacement, the floor absolute acceleration, and the overturning moment. "Main" and "Sub" shown in Figures 12 and 13 represent the main structure and substructure of DSO. As seen from these figures, it is observed that the control effectiveness of DSO and DO are surprising. However, the larger value of β commonly contributes less reduction for structural response. For instance, the damping effectiveness of DO for $\beta = 0.5$ outperforms that of $\beta = 2$, and the similar results can only be found for DSO in overturning moment. In addition, as $\beta = 0.5$ shown in Figure 12(a), the seismic reduction of core tube for DO is better than that of DSO in floor displacement. Interestingly, compared by Figures 12(a) and 13(a), DSO has less change in control effectiveness than that of DO for $\beta = 2$, suggesting the superiority of the proposed novel outrigger system. In other word, DSO has strong robustness to β in floor displacement control. Moreover, the response for substructures of DSO can be reduced a lot, but the 1st substructure may amplify the response. Note that the structural safety of the main structure should be considered as the most important factor, and hence an appropriate sacrifice of the control performance for substructures is not necessarily a bad thing. As for floor absolute acceleration shown in Figures 12(b) and 13(b), although there is no evident changing regularity, both DSO and DO perform well. To give the time history of the top response, Figure 14 shows the top response for $f_s = 2.5$, $\beta = 2$ under El Centro, in which a peak reduction of 30.57% in displacement and 47.64% in absolution acceleration can be observed for DSO, while 25.76% and 25.42% for those of DO. Similarly, the peak reductions of top response under Northrige are 16.64% and 58.70% for DSO in displacement and absolution acceleration, while 12.62% and 23.36% for those of DO.

Most importantly, as shown in Figures 12(c) and 13(c), when compared to DO, the greater advantages in reduction of overturning moment can be found for DSO; Moreover, the larger value of β, such as $\beta = 2$, shows less impacts on the control effectiveness of overturning moment. Thus, it is indisputable that DSO possesses superiority in the suppression of structural vibration, particularly the overturning moment and structural response under larger β.

Harmful interstory drift ratio is one of the important safety indexes [30, 31]. Figure 15 shows the harmful interstory drift comparisons under El Centro and Northrige records. It can be seen that β also significantly impacts on the reduction of harmful interstory drift ratio. The influence of β on DO is more significant than that on mian structure of DSO. For example, DO can reduce the half and even less seismic response of TO in interstory drift ratio when $\beta = 0.5$, while this case degenerates a lot when $\beta = 2$. Fortunately, DSO greatly improves above situations and presents the better control effect. However, the substructures perform less control effect in harmful interstory drift ratio when compared with those of main structure, especially for the lower substructures. This is because the total vibration energy is adopted as the optimization objective. Besides, those substructures are partly independent and more vibration energy may transfer to them as mentioned in Section 3. However, this case could be improved through multi-objective optimization.

4.2. Structural Energy Analysis. To further investigate seismic performance, the energy response comparisons, such as input energy, kinetic energy, and damper dissipation energy, are plotted in Figures 16–19. Figure 16 shows the input energy comparison under El Centro and Northrige records. It is observed that when $\beta = 0.5$, DSO can reduce the input energy by 31.16% compared to that of TO under El Centro record and it is slightly less than that of DO with 47.37%. Meanwhile, DSO can also reduce the input energy by 2.90% compared to that of TO under Northrige record, and it is significantly less than that of DO with 39.61%. Such results indicate that these two controlled outrigger systems can effectively reduce the input energy, and DO outperform DSO. However, when $\beta = 2$, DO amplifies the input energy of TO by 20.27% under El Centro record, and that of DSO is 25.05%. Meanwhile, both DO and DSO under Northrige record amplify the input energy of TO by 47.16% and 62.47%, respectively. In view of this, the larger value of β is against the reduction of input energy and the difference in the reduction of input energy between DO and DSO has narrowed. Mostly, Figure 18 indicates that not only DO but also DSO can significantly suppress the structural vibration and reduce the kinetic energy under the selected two ground motions. Moreover, though the input energy of DO and DSO under Northrige record (Figure 16(d)) is amplified when $\beta = 2$, these two control systems can effectively reduce the kinetic energy. For example, the maximum kinetic energy of DO is 1.17×10^7 J and that of DSO is 1.40×10^7 J, and hence they contribute the energy reduction of 34.85% and 22.46% to that of TO (1.81×10^7 J). In addition, DSO under

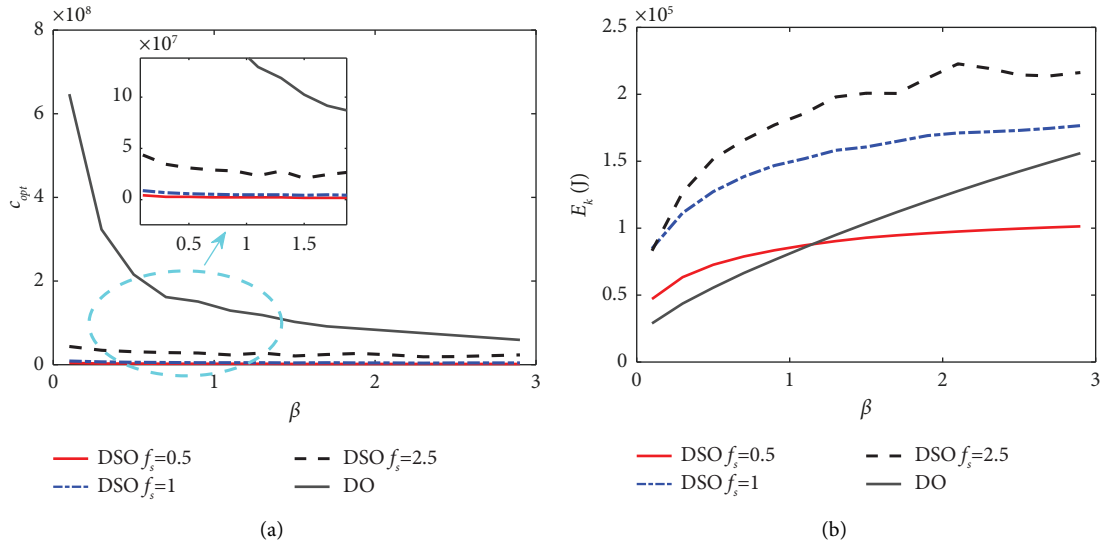

FIGURE 11: c_{opt} and the corresponding total vibration energy (u = 1). (a) c_{opt} versus β and f_s. (b) E_k versus β and f_s with c_{opt}.

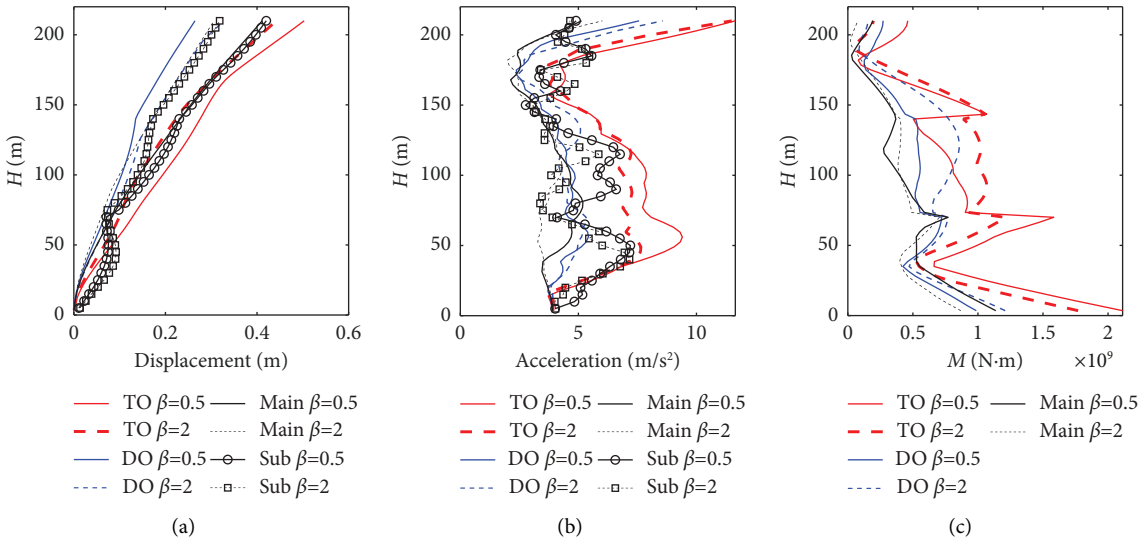

FIGURE 12: Structural responses under El Centro: (a) floor displacement; (b) floor absolute acceleration; (c) overturning moment.

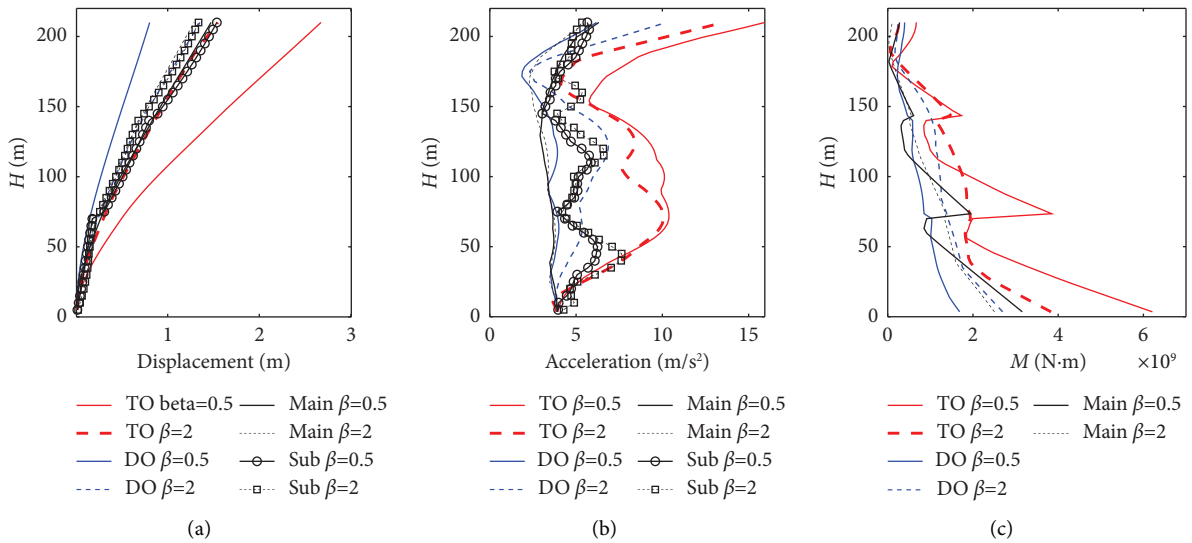

FIGURE 13: Structural responses under Northrige: (a) floor displacement; (b) floor absolute acceleration; (c) overturning moment.

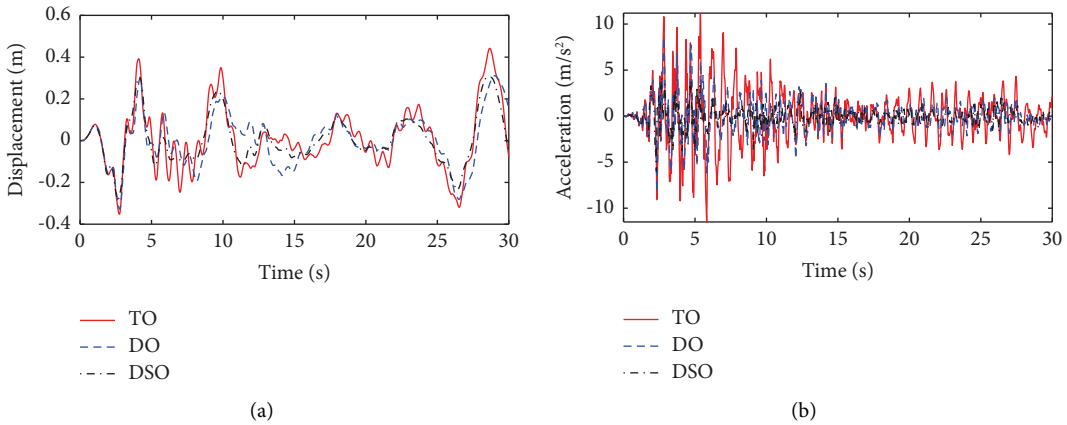

Figure 14: Top response under El Centro ($\beta = 2$): (a) displacement; (b) absolute acceleration.

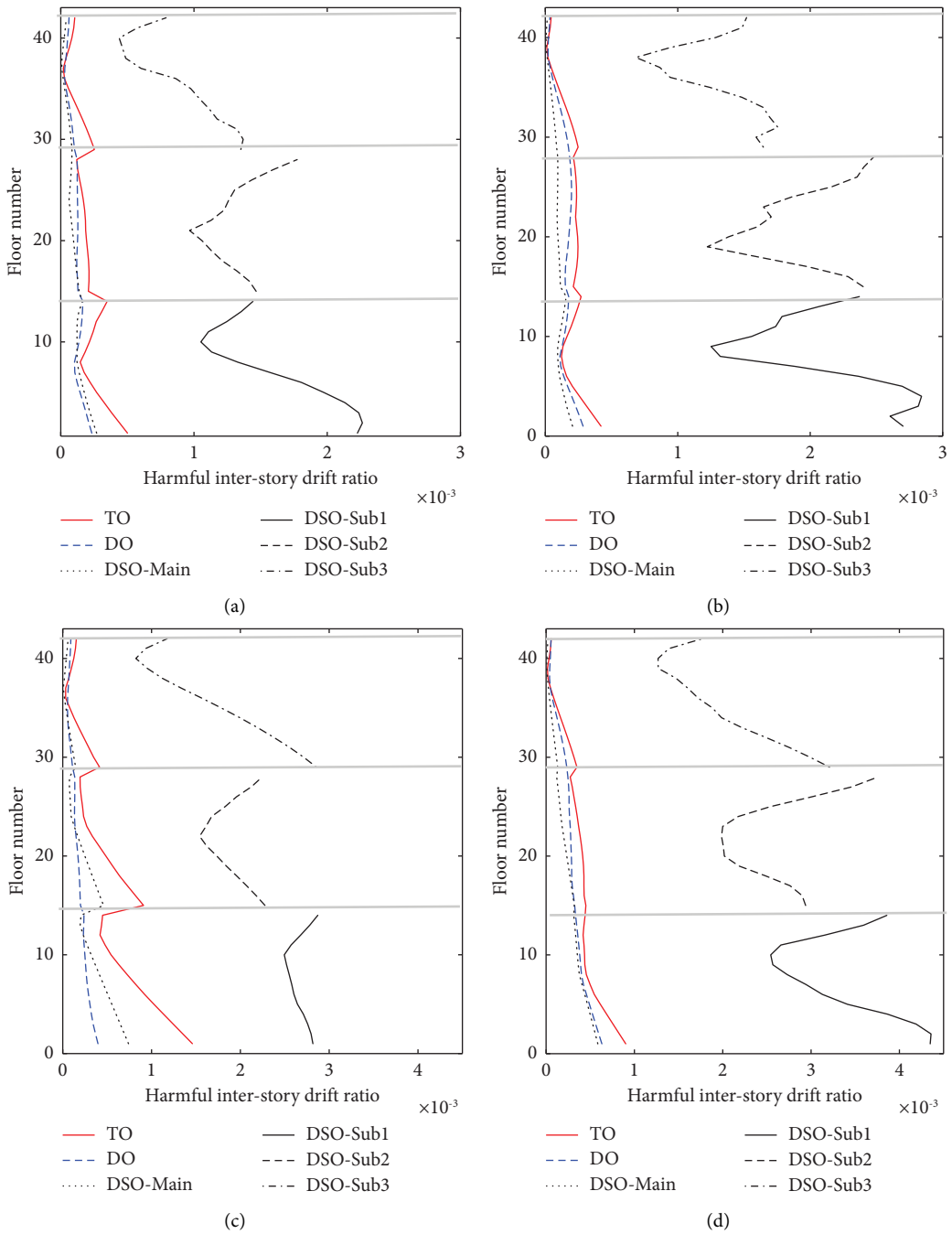

Figure 15: Interstory drift comparisons: (a) El Centro ($\beta = 0.5$); (b) El Centro ($\beta = 2$); (c) Northrige ($\beta = 0.5$); (d) Northrige ($\beta = 2$).

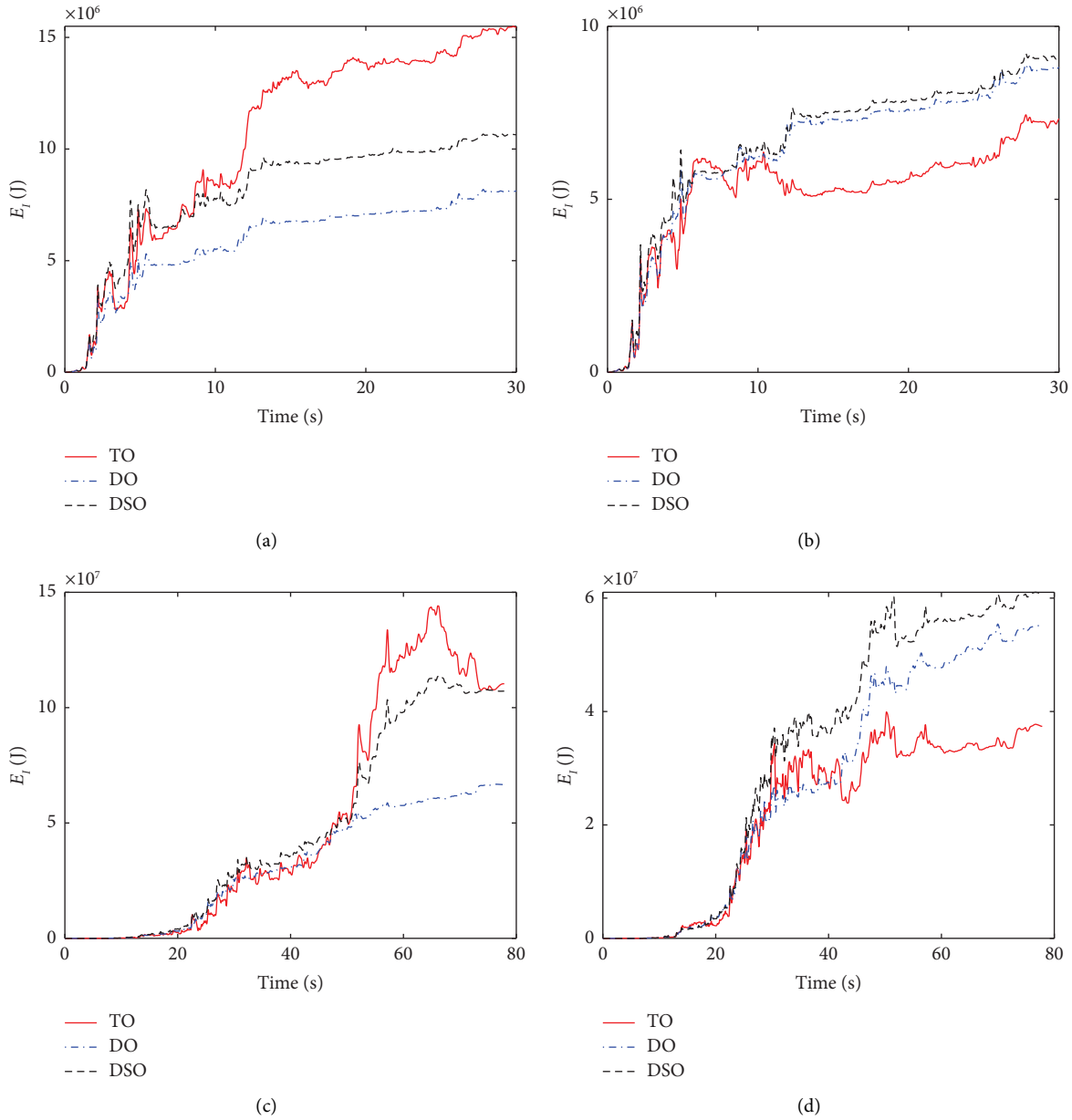

Figure 16: Input energy comparison (El Centro): (a) $\beta = 0.5$ (El Centro). (b) $\beta = 2$ (El Centro). (c) $\beta = 0.5$ (Northrige). (d) $\beta = 2$ (Northrige).

El Centro shows almost no difference from DO in kinetic energy reduction when $\beta = 2$. Therefore, the kinetic energy reduction sensitivity of DSO to β is lower than that of DO, i.e., DSO may behaves relatively stable damping performance.

For simplicity, the energy distributions of each substructure under El Centro record are shown in Figure 19. As shown in Figure 19, DSO displays a special ability in that the kinetic energy can be well-distributed to all parts of the structure. For example, as shown in Figure 19(a), the more kinetic energy has been transferred to substructures (particularly for 3rd substructure), and hence the main structure possesses less than 50% of the total kinetic energy. For another example, as shown in Figure 19(b), the more kinetic energy has also been transferred to substructures (particularly for 2nd and 3rd substructures), and less percent of the total kinetic energy of the main structure can be found for that of $\beta = 2$. Generally, though DSO possesses a slightly more total kinetic energy than DO (Figure 18), the distribution of the total kinetic energy for DSO is relatively uniform, and the structural safety can be guaranteed due to less energy concentration on the certain part. In other words, the above energy distribution of DSO is good for structural safety due to a lot of kinetic energy transferred to the substructure, and hence the main structure is actually in a safe state.

The damper dissipation energy is a critical factor for structural damping performance, and the corresponding energy comparison under El Centro plotted in Figure 17. As seen in Figure 17, "Ed" represents the total dissipation

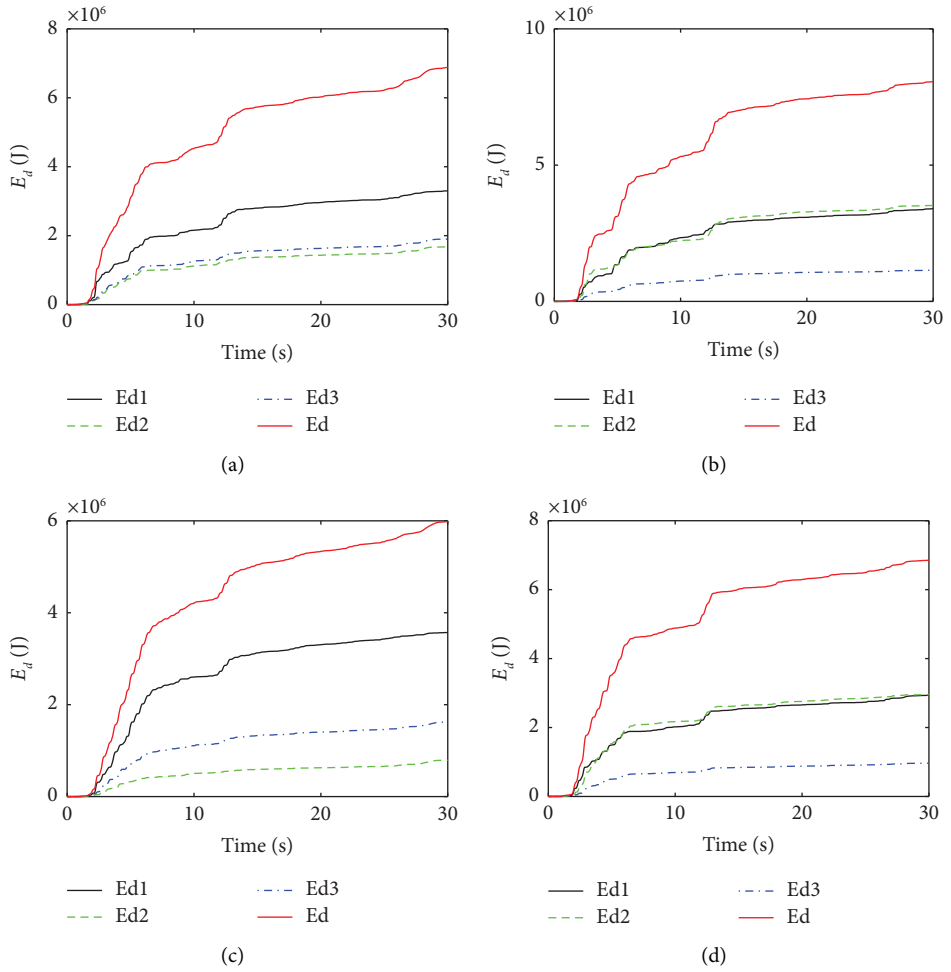

Figure 17: Damper dissipation energy comparison (El Centro): (a) DO ($\beta = 0.5$); (b) DSO ($\beta = 0.5$); (c) DO ($\beta = 2$); (d) DSO ($\beta = 2$).

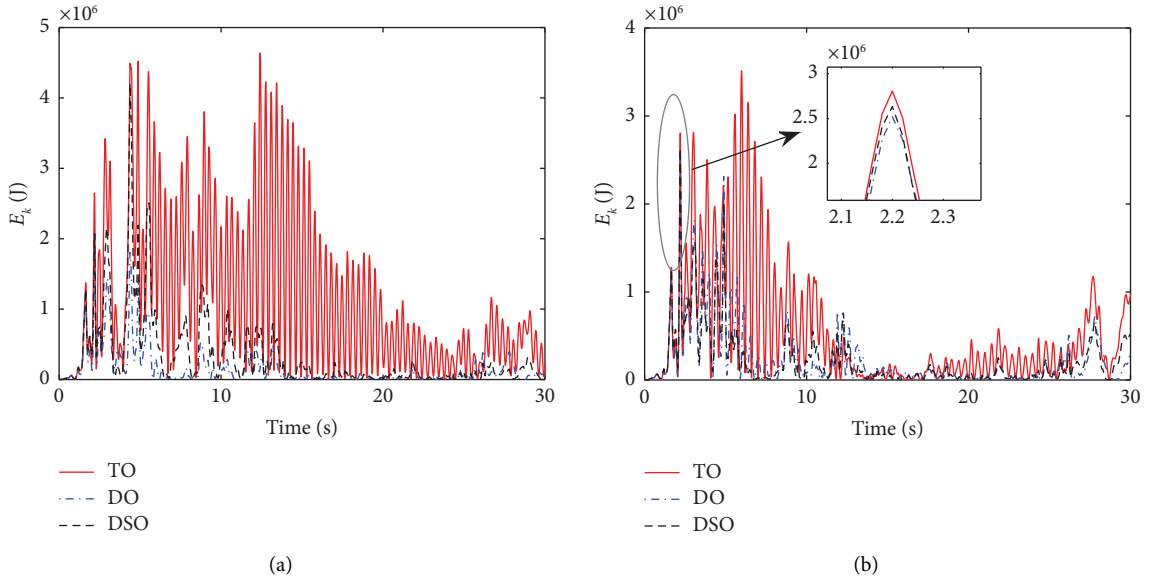

Figure 18: Continued.

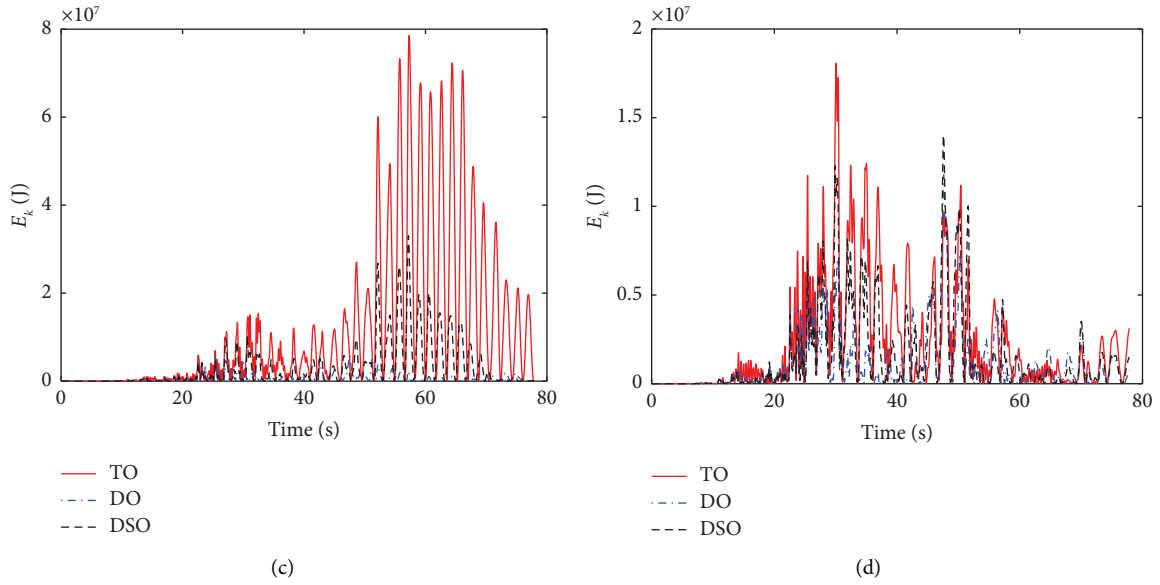

Figure 18: Kinetic energy comparison. (a) $\beta = 0.5$ (El Centro). (b) $\beta = 2$ (El Centro). (c) $\beta = 0.5$ (Northrige). (d) $\beta = 2$ (Northrige).

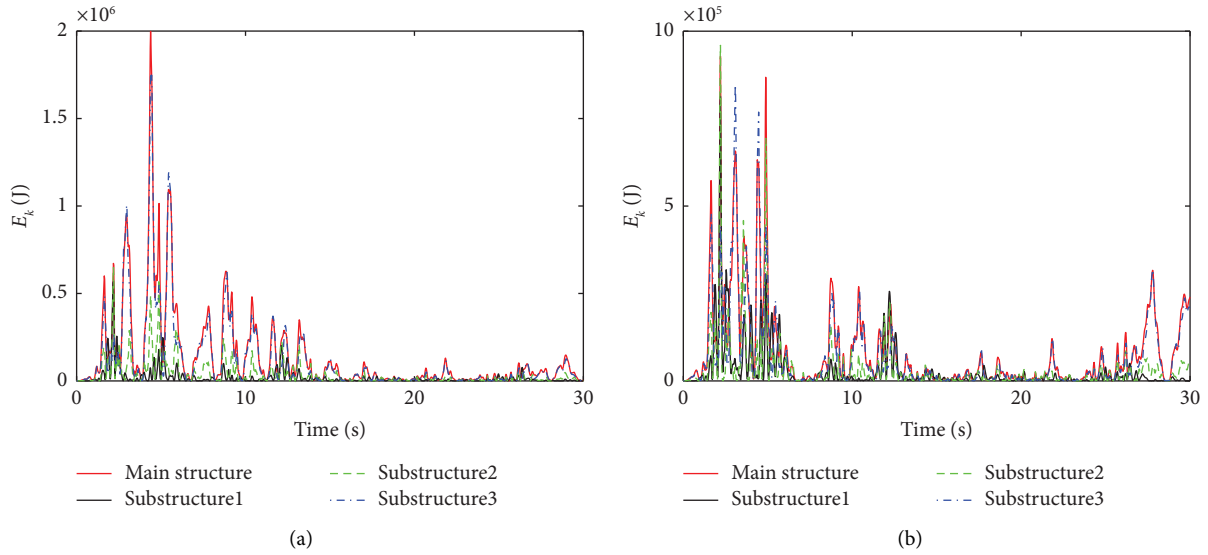

Figure 19: Kinetic energy for each part of DSO (El Centro): (a) $\beta = 0.5$; (b) $\beta = 2$.

energy, and "Edj" represents the dissipation energy of all dampers close to the jth outrigger. In addition, each outrigger of DO has two dampers, and twice times of damping force are included; meanwhile, one damper for DSO (Figure 6). As shown in Figures 17(a) and 17(b) ($\beta = 0.5$), DSO and DO dissipate 75.81% and 84.66% of input energy, respectively. Similarly, as shown in Figures 17(c) and 17(d) ($\beta = 2$), DSO dissipates 74.80% of input energy and outperforms that of DO for 67.80%. Thus, even for the larger stiffness ratio, such as $\beta = 2$, DSO still maintains a high damping efficiency when compared to DO. The above results are attributed to the larger relative deformation between the substructure and the main structure, and thus the accompanying damping performance is well improved. Besides, note that such deformation is far larger that the "one story" deformation. In addition to this, the force-displacement curves under El Centro shown in Figures 20 and 21 can also give the explanations for the aforementioned

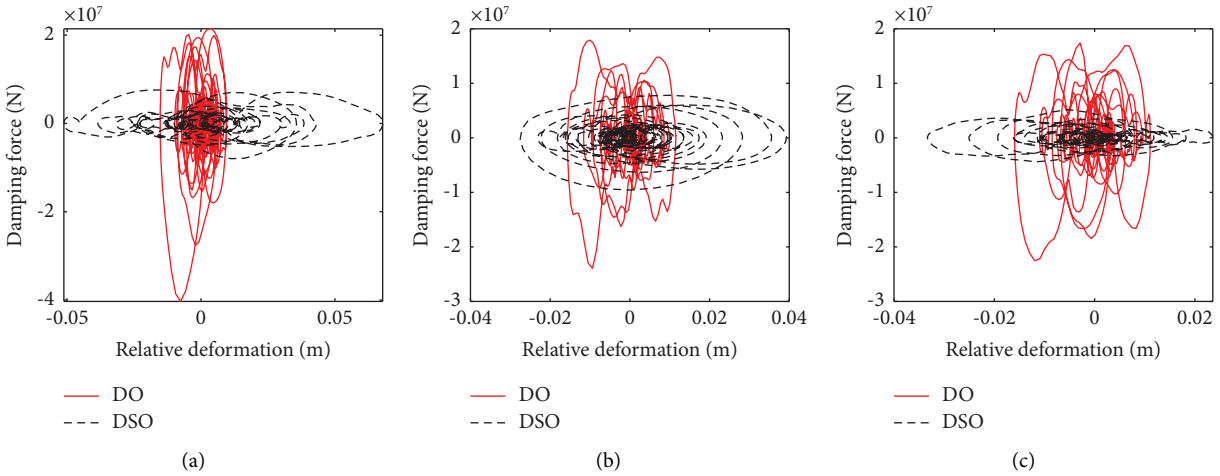

FIGURE 20: Force-displacement curves under El Centro ($f_s = 2.5$, $\beta = 0.5$): (a) 1st outrigger; (b) 2nd outrigger; (c) 3rd outrigger.

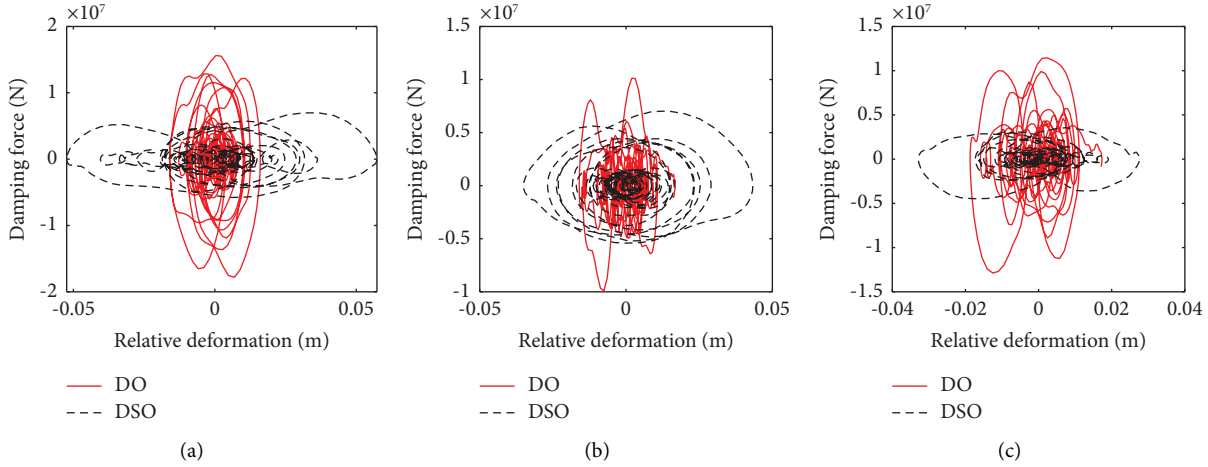

FIGURE 21: Force-displacement curves under El Centro ($f_s = 2.5$, $\beta = 2$): (a) 1st outrigger; (b) 2nd outrigger; (c) 3rd outrigger.

results. As seen in Figures 20 and 21, when compared with the DO, although the smaller damping force is produced by DSO, the larger stroke of the viscous damper can be obtained. More importantly, combing Figures 11, 17, 20 and 21, it is true that DSO achieves the higher efficiency in energy dissipation but only depends on less damping of the viscous damper. Therefore, there is no doubt that the above results indicate the superiority of the proposed novel outrigger system.

5. Conclusions

A novel outrigger system, the damped substructure outrigger tall building (DSO), is proposed to improve damping performance. This system possesses good structural integrity due to the main structure consisted of the core tube, outrigger, and perimeter column. With the several efforts, DSO is essentially simplified to be a cantilever beam system with a multirotation spring and energy dissipation substructure. Based on the simplified model, the corresponding vibration differential equations are derived. Then, further energy distribution regularity and seismic performance have been investigated. Conclusions are summarized as follows:

(1) DSO shows well-controlled performance in vibration energy reduction. But the perimeter column stiffness ratio β behaves significant impact on vibration energy, and the smaller value of β contributes better performance and needs a larger value of λ_{opt}.

(2) The main structure of DSO not only has the lower energy but also locates in a lower energy proportion. In other words, the main structure can keep in a relatively safe state and the substructure is easier to break first. This mechanism is critical to structural safety performance.

(3) Frequency ratio f_s significantly affects the total vibration energy and the smaller f_s leads to the lower vibration energy but more sensitive to λ. Besides, the smaller of f_s results in lower total vibration energy and vibration energy ratio of main structure when λ_{opt} is adopted.

(4) The analytical results point out the superiority of DSO in seismic response reduction. Although the larger β commonly contributes less reduction for structural response, DSO has less degeneration in control effectiveness than that of DO. Generally, DSO possesses superiority in the suppression of structural vibration, particularly the overturning moment and structural response when larger β is adopted.

(5) Compared with DO, DSO can also obtain the same high efficiency in energy dissipation but with less damping cost of the viscous damper. Moreover, the larger stroke of the viscous damper can be found for DSO.

Data Availability

The data that support the findings of this study are available from the corresponding author upon request.

Conflicts of Interest

The authors declare that they have no conflicts of interest.

Acknowledgments

The authors are grateful for the financial support received from the National Natural Science Foundation of China (Grant no. 51908129), Foundation for Distinguished Young Talents in Higher Education of Guangdong (Grant no. 2021KQNCX096), Guangdong Basic and Applied Basic Research Foundation (Grant nos. 2020A1515110806, 2020A1515110573, and 2021A1515110677), and Guangdong-Macau Joint Funding Topic of Science and Technology Innovation (2022A0505020030).

References

[1] B. Kavyashree, S. Patil, and V. S. Rao, "Evolution of outrigger structural system: a state-of-the-art review," *Arabian Journal for Science and Engineering*, vol. 46, no. 11, pp. 10313–10331, 2021.

[2] I. Netzer and O. Lavan, "Optimized seismic design of passively damped outriggers considering perimeter column flexibility," *Journal of Structural Engineering*, vol. 146, no. 12, Article ID 04020254, 2020.

[3] M. M. Ali and K. S. Moon, "Structural developments in tall buildings: current trends and future prospects," *Architectural Science Review*, vol. 50, no. 3, pp. 205–223, 2007.

[4] J. R. Wu and Q. S. Li, "Structural performance of multi-outrigger-braced tall buildings," *The Structural Design of Tall and Special Buildings*, vol. 12, no. 2, pp. 155–176, 2003.

[5] E. Brunesi, R. Nascimbene, and L. Casagrande, "Seismic analysis of high-rise mega-braced frame-core buildings," *Engineering Structures*, vol. 115, pp. 1–17, 2016.

[6] J. Lee, M. Bang, and J. Y. Kim, "An analytical model for high-rise wall-frame structures with outriggers," *The Structural Design of Tall and Special Buildings*, vol. 17, no. 4, pp. 839–851, 2008.

[7] L. Liu, X. Li, P. Tan, Z. Pan, and S. Zhang, "Damping performance analysis of the damped outrigger system based on H," *International Journal of Structural Stability and Dynamics*, vol. 22, no. 13, Article ID 2250149, 2022.

[8] J.-G. Nie, R. Ding, J.-S. Fan, and M.-X. Tao, "Seismic performance of joints between steel K-style outrigger trusses and concrete cores in tall buildings," *Journal of Structural Engineering*, vol. 140, no. 12, Article ID 04014100, 2014.

[9] L. Xing, Y. Zhou, and M. Aguaguiña, "Optimal outrigger locations of double-pure-outrigger systems and combined energy-dissipating outrigger systems under seismic loads," *Soil Dynamics and Earthquake Engineering*, vol. 153, Article ID 107121, 2022.

[10] C.-M. Chang, Z. Wang, B. F. Spencer, and Z. Chen, "Semi-active damped outriggers for seismic protection of high-rise buildings," *Smart Structures and Systems*, vol. 11, no. 5, pp. 435–451, 2013.

[11] B. S. Smith and I. Salim, "Parameter study of outrigger-braced tall building structures," *Journal of the Structural Division*, vol. 107, no. 10, pp. 2001–2014, 1981.

[12] P. Tan, C. Fang, and F. Zhou, "Dynamic characteristics of a novel damped outrigger system," *Earthquake Engineering and Engineering Vibration*, vol. 13, no. 2, pp. 293–304, 2014.

[13] T. Yang, J. Atkinson, L. Tobber, D. P. Tung, and B. Neville, "Seismic design of outrigger systems using equivalent energy design procedure," *The Structural Design of Tall and Special Buildings*, vol. 29, no. 10, p. e1743, 2020.

[14] Y. Zhou, C. Zhang, and X. Lu, "Seismic performance of a damping outrigger system for tall buildings," *Structural Control and Health Monitoring*, vol. 24, no. 1, Article ID e1864, 2017.

[15] Y. Zhou and H. Li, "Analysis of a higherformance of a damping outrigger system for tall buildings," *Structural Control and Health Monitoring*, vol. 24, pp. e1864.3–79, 2017.

[16] F.-F. Sun, M. Wang, and S. Nagarajaiah, "Multi-objective optimal design and seismic performance of negative stiffness damped outrigger structures considering damping cost," *Engineering Structures*, vol. 229, Article ID 111615, 2021.

[17] S. Nagarajaiah, "Adaptive passive, semiactive, smart tuned mass dampers: identification and control using empirical mode decomposition, hilbert transform, and short-term fourier transform," *Structural Control and Health Monitoring*, vol. 16, no. 7-8, pp. 800–841, 2009.

[18] Y. Chen, D. McFarland, Z. Wang, B. Spencer, and L. Bergman, "Analysis of tall buildings with damped outriggers," *Journal of Structural Engineering*, vol. 136, no. 11, pp. 1435–1443, 2010.

[19] B. Huang and T. Takeuchi, "Dynamic response evaluation of damped-outrigger systems with various heights," *Earthquake Spectra*, vol. 33, no. 2, pp. 665–685, 2017.

[20] R. J. Smith and M. R. Willford, "The damped outrigger concept for tall buildings," *The Structural Design of Tall and Special Buildings*, vol. 16, no. 4, pp. 501–517, 2007.

[21] Z. Wang, Y. Zhou, C. Fang, and J. Zhang, "Stochastic optimization and sensitivity analysis of the combined negative stiffness damped outrigger and conventional damped outrigger systems subjected to nonstationary seismic excitation," *Structural Control and Health Monitoring*, vol. 2023, Article ID 4024741, 2023.

[22] S. Al-Subaihawi, C. Kolay, T. Marullo, J. M. Ricles, and S. E. Quiel, "Assessment of wind-induced vibration mitigation in a tall building with damped outriggers using real-time hybrid simulations," *Engineering Structures*, vol. 205, Article ID 110044, 2020.

[23] S. E. Quiel, C. Kolay, J. M. Ricles, T. M. Marullo, and S. Al Subaihawi, "Multi-hazard real-time hybrid simulation of a tall building with damped outriggers," *International Journal of Lifecycle Performance Engineering*, vol. 4, no. 1/2/3, pp. 103–132, 2020.

[24] K. Park, D. Kim, D. Yang, D. Joung, I. Ha, and S. Kim, "A comparison study of conventional construction methods and outrigger damper system for the compensation of differential column shortening in high-rise buildings," *International Journal of Steel Structures*, vol. 10, no. 4, pp. 317–324, 2010.

[25] M. R. Willford, R. J. Smith, D. Scott, and M. Jackson, "Viscous dampers come of age," *Structures Magazine*, vol. 6, pp. 15–18, 2008.

[26] J. Ding, S. Wang, and H. Wu, "Seismic performance analysis of viscous damping outrigger in super high-rise buildings," *The Structural Design of Tall and Special Buildings*, vol. 27, no. 13, p. e1486, 2018.

[27] Z. Lu, X. He, and Y. Zhou, "Performance-based seismic analysis on a super high-rise building with improved viscously damped outrigger system," *Structural Control and Health Monitoring*, vol. 25, no. 8, Article ID e2190, 2018.

[28] P. Tan, C. Fang, W. Tu, F. Zhou, Y. Wang, and M. Jiang, "Experimental study on the outrigger damping system for high-rise building," in *Proceedings of the 15th World Conference on Earthquake Engineering*, Lisbon, Portugal, June 2012.

[29] C. Fang, "Applicability of damped outrigger systems using timoshenko beam theory," *International Journal of Structural Stability and Dynamics*, vol. 22, no. 6, Article ID 2250076, 2022.

[30] C. Fang, B. Spencer, J. Xu, P. Tan, and F. Zhou, "Optimization of damped outrigger systems subject to stochastic excitation," *Engineering Structures*, vol. 191, pp. 280–291, 2019.

[31] M. Wang, S. Nagarajaiah, and F.-F. Sun, "Optimal design of supplemental negative stiffness damped outrigger system for high-rise buildings resisting multi-hazard of winds and earthquakes," *Journal of Wind Engineering and Industrial Aerodynamics*, vol. 218, Article ID 104761, 2021.

[32] M. Wang, S. Nagarajaiah, and F.-F. Sun, "Dynamic characteristics and responses of damped outrigger tall buildings using negative stiffness," *Journal of Structural Engineering*, vol. 146, no. 12, Article ID 04020273, 2020.

[33] M. Wang, S. Nagarajaiah, and F.-F. Sun, "A novel crosswind mitigation strategy for tall buildings using negative stiffness damped outrigger systems," *Structural Control and Health Monitoring*, vol. 29, no. 9, p. e2988, 2022.

[34] Y. Xiang, P. Tan, H. He, and Q. Chen, "Seismic optimization for hysteretic damping-tuned mass damper (hd-tmd) subjected to white-noise excitation," *Structural Control and Health Monitoring*, vol. 2023, Article ID 1465042, 2023.

[35] M. Wang, F.-F. Sun, Y. Koetaka, L. Chen, S. Nagarajaiah, and X.-L. Du, "Frequency independent damped outrigger systems for multi-mode seismic control of super tall buildings with frequency independent negative stiffness enhancement," *Earthquake Engineering & Structural Dynamics*, vol. 52, no. 9, pp. 2731–2754, 2023.

[36] L. Liu, P. Tan, H. Ma, W. Yan, and F. Zhou, "A novel energy dissipation outrigger system with rotational inertia damper," *Advances in Structural Engineering*, vol. 21, no. 12, pp. 1865–1878, 2018.

[37] H. Beiraghi, "Near-fault ground motion effects on the responses of tall reinforced concrete walls with buckling-restrained brace outriggers," *Scientia Iranica*, vol. 25, pp. 1987–1999, 2018.

[38] P. C. Lin, T. Takeuchi, and R. Matsui, "Seismic performance evaluation of single dampedced concrete walls with buckling-restrained brace outriggers," *Scientia Iranica*, vol. 25, pp. 1987–1999, 2018.

[39] L. Xing, Y. Zhou, and M. Aguaguiña, "Optimal vertical configuration of combined energy dissipation outriggers," *The Structural Design of Tall and Special Buildings*, vol. 28, no. 4, p. e1579, 2019.

[40] R. Mirza Hessabi and O. Mercan, "Investigations of the application of gyro-mass dampers with various types of supplemental dampers for vibration control of building structures," *Engineering Structures*, vol. 126, pp. 174–186, 2016.

[41] J.-S. Hwang, Y.-N. Huang, and Y.-H. Hung, "Analytical and experimental study of toggle-brace-damper systems," *Journal of Structural Engineering*, vol. 131, no. 7, pp. 1035–1043, 2005.

[42] A. N. Şigaher and M. C. Constantinou, "Scissor-jack-damper energy dissipation system," *Earthquake Spectra*, vol. 19, no. 1, pp. 133–158, 2003.

[43] H. Tagawa, T. Yamanishi, A. Takaki, and R. W. Chan, "Cyclic behavior of seesaw energy dissipation system with steel slit dampers," *Journal of Constructional Steel Research*, vol. 117, pp. 24–34, 2016.

[44] X. Li, P. Tan, Y. Wang et al., "Shaking table test and numerical simulation on a mega-sub isolation system under near-fault ground motions with velocity pulses," *International Journal of Structural Stability and Dynamics*, vol. 22, no. 2, Article ID 2250026, 2022.

[45] X. Zhang, X. Qin, S. Cherry, Y. Lian, J. Zhang, and J. Jiang, "A new proposed passive mega-sub controlled structure and response control," *Journal of Earthquake Engineering*, vol. 13, no. 2, pp. 252–274, 2009.

[46] Y. Xu, Q. He, and J. Ko, "Dynamic response of damper-connected adjacent buildings under earthquake excitation," *Engineering Structures*, vol. 21, no. 2, pp. 135–148, 1999.

[47] H. Zhu, D. Ge, and X. Huang, "Optimum connecting dampers to reduce the seismic responses of parallel structures," *Journal of Sound and Vibration*, vol. 330, no. 9, pp. 1931–1949, 2011.

[48] H. Zhu, Y. Wen, and H. Iemura, "A study on interaction control for seismic response of parallel structures," *Computers & Structures*, vol. 79, no. 2, pp. 231–242, 2001.

[49] P. Tan, C. Fang, C. Chang, B. Spencer, and F. Zhou, "Dynamic characteristics of novel energy dissipation systems with damped outriggers," *Engineering Structures*, vol. 98, pp. 128–140, 2015.